SPE 110858

Gas Production From Class 2 Hydrate Accumulations in the Permafrost

George J. Moridis, SPE, and Matthew T. Reagan, SPE, Lawrence Berkeley National Laboratory

Abstract

Gas hydrates are solid crystalline compounds in which gas molecules are lodged within the lattices of ice crystals. Natural hydrates in geological systems are composed mainly of methane. The amounts of hydrocarbon gases trapped in natural hydrate accumulations are enormous, leading to a recent interest in the evaluation of their potential as an energy source.

Class 2 hydrate deposits are characterized by a Hydrate-Bearing Layer (HBL) underlain by a saturated zone of mobile water, and are encountered in the permafrost and in deep ocean sediments. The base of the HBL in Class 2 deposits may occur at the edge of, or within, the zone of thermodynamic hydrate stability. Because of the manner of their formation from pre-existing gas reservoirs, permafrost hydrate deposits are generally characterized by high hydrate saturations and are bounded by relatively impermeable strata.

In this numerical study of long-term gas production from permafrost-associated (PA) Class 2 deposits, we investigate three different well configurations that involve different production intervals and combinations of depressurization (the main dissociation-inducing mechanism) with localized thermal stimulation. Using fine grids and realistic production scenarios, we determine that large volumes of gas can be produced at high rates (several MMSCFD) for long times using conventional technology. The production approach involves initial fluid withdrawal from the water zone underneath the HBL. The production process follows a cyclical pattern, with each cycle composed of two stages: a long stage (months to years) of increasing gas production and decreasing water production, and a short stage (days to weeks) that involves destruction of the secondary hydrate (mainly though warm water injection) that evolves during the first stage, and is followed by a reduction in the fluid withdrawal rate. A well configuration that initially involves heating of the outer surface of the wellbore and later continuous injection of warm water at low rates appears to deliver optimum performance over the period it takes for the exhaustion the hydrate deposit. We determine that gas production is affected by the well design, and increases with the fluid withdrawal rate and the initial hydrate saturation.

Introduction

Background. Gas hydrates are solid crystalline compounds in which gas molecules (referred to as guests) occupy the lattices of ice crystal structures (called hosts). Natural hydrates in geological systems usually contain CH_4 as their main gas ingredient, and occur in two distinctly different geologic settings where the necessary conditions of low T and high P exist for their formation and stability: in the permafrost and in deep ocean sediments.

Although the range of current estimates of the size of the hydrocarbon resource trapped in hydrates is very wide[1,2,3] (ranging between 10^{15} to 10^{18} ST m^3), there is general agreement that it is vast and that it exceeds the total energy content of the known conventional fossil fuel resources. Even if the most conservative estimate is considered, and if only a fraction of the resource is recoverable, the magnitude of the resouce is sufficiently large to attract attention as a potential energy source[4,5], given the ever increasing global energy demand, the dwindling conventional fossil hydrocarbon reserves, and the environmental desirability of CH_4 as a fuel. To that end, there has been a proliferation of recent studies evaluating the technical and economic feasibility of gas production from natural hydrate accumulations.[5-11]

Dissociation methods. Gas can be produced from hydrates by inducing dissociation by one of the three main dissociation methods[12] (or combinations thereof): (1) depressurization, involving lower of the pressure P below the hydration pressure P_e (as defined by the Lw-H-V and I-H-V three-phase lines in Figure 1) at the temperature T, (2) thermal stimulation, based on raising T above the hydration temperature T_e at the prevailing P, and (3) the use of inhibitors (such as salts and alcohols), which shifts the P_e-T_e equilibrium through competition with the hydrate for guest and host molecules.

Characteristics of Class 2 hydrate deposits in the permafrost. Natural hydrate accumulations are divided into four main classes.[6-9] Class 2 accumulations are bounded by confining strata (overburden and underburden), and are composed of two layers: the Hydrate-Bearing Layer (hereafter referred to as HBL) and an underlying zone of mobile water (hereafter referred to as WZ). In this type of hydrate accumulation, the bottom of the hydrate stability zone (i.e., the location above which hydrates are stable because of thermodynamically favorable P and T conditions, as indicated by the Lw-H-V and I-H-V lines in Figure 1) may occur at or below the bottom of the hydrate interval. Thus, the entire HBL may be well within the hydrate stability zone and can exist under equilibrium or stable conditions. Proximity of the base of the HBL to the bottom of the hydrate stability zone (which defines equilibrium and is characterized by the maximum possible temperature $T = T_e$ at the prevailing P) enhances the gas production potential of the deposit because of the larger sensible heat reservoir at the higher T (available to support the endothermic dissociation reaction), in addition to the ease of destabilizing the hydrate in the vicinity of thermodynamic equilibrium[7].

Class 2 deposits are quite common both in the permafrost[5] and in the oceans[7], and there is geologic, geochemical and thermodynamic justification for the expectation that they are probably the most prevalent type among the hydrate deposits that are potential production targets.

There are two differences between oceanic and Class 2 PA accumulations. The first difference is obviously the relatively low concentrations of salt (an inhibitor) in the majority of PA deposits[5,13], which are generally insufficient to cause a substantial shift in the P_e -T_e equilibrium. For example, at a temperature T_e = 13 ^oC, the equilibrium hydration pressure P_e = 12.24 MPa in a typical marine deposit with a water salinity of X_S = 3.5%, but is only P_e = 10.26 MPa in a PA deposit with X_S = 0.35%, and P_e = 10.07 MPa for X_S = 0. Consequently, depressurization-induced gas production is more difficult in PA deposits because it is deprived of the beneficiary effect of salt. This means lower and delayed gas production because larger pressure drops ΔP (requiring larger fluid withdrawal rates and/or longer production periods) are needed to effect the same gas production.

The second difference involves the initial P and T in Class 2 deposits, as determined by their location in the subsurface. Barring very large abnormalities in the geothermal gradient, the deepest interface in Class 2 PA deposits occurs at a depth of about 1150-1200 m, with corresponding P and T not exceeding 11.3 – 11.8 MPa (= 1640 – 1700 psi) and about 14 ^oC, respectively). Conversely, oceanic Class 2 deposits can be encountered at practically any depth below a minimum threshold, and very deep such deposits have been reported[7]. Deeper deposits are characterized by larger P and T (as they generally follow the hydrostatic and the geothermal gradients), making them more desirable targets because of (a) a larger depressurization ΔP potential, and (b) a larger sensible heat reservoir to support the endothermic dissociation reaction. Given the fixed maximum depth of hydrate deposits in the permafrost and the general desirability of deeper, warmer deposits as production targets, the deepest PA accumulations appear to be less promising than the deepest oceanic ones because of lower P and T (reflecting the combined effect of the shallower depth and the influence of permafrost). Note that this evaluation is based on the production potential of these two deposit types, and does not account for the considerable technical and economic challenges of offshore operations.

A practical implication of the generally lower P and T in permafrost Class 2 deposits is a limitation on the mass rate of fluid withdrawal from the well Q_M to effect depressurization, and, consequently, on the rate of gas production Q_P. This limitation is not imposed by permeability restrictions but by concerns about the possible emergence of ice, which can have a very adverse impact on the effective permeability k_{eff}. Thus, given the fact that the heat of hydrate dissociation ΔH is practically unaffected by T and the sensible heat reservoir is smaller in the colder PA deposits, a relatively low Q_M is necessary to maintain T above freezing. For a given hydrate saturation S_H, the low Q_M limits the rate of cooling brought about by dissociation and the Joule-Thompson effect, while allowing heat inflows through the boundaries to replenish the heat losses. Much higher Q_M rates are possible in deeper, warmer Class 2 oceanic deposits with the same geometry, S_H, and intrinsic permeability k.

Production from oceanic Class 2 deposits was discussed in detail by *Moridis and Reagan*.[7] Although there have been earlier studies of gas production from permafrost Class 2 deposits[10.14,15], these were exploratory in nature because they did not have the benefit of recent advances in our understanding of the thermal and hydraulic behavior of hydrate-bearing geologic media.[16,17] Thus, the results of the earlier studies provided important insights into the system behavior through the sensitivity analysis of the factors affecting gas production from Class 2 deposits, but they had mainly qualitative value (in the sense of providing indications of relative performance).

Objective and approach. The main objective of this study is to evaluate the production potential of Class 2 PA accumulations, and to determine the factors and conditions affecting it. As discussed in detail by *Moridis and Reagan*[7,8], depressurization appears to be the production method of choice for the following reasons: its simplicity, its technical and economic effectiveness, the fast response of hydrates to the rapidly propagating pressure wave, the near-incompressi-bility of water (which expands the volume over which depressurization is sensed by the HBL), and the large heat capacity of water. The latter plays a significant role in providing part of the heat needed to support the strongly endothermic dissociation reaction as warmer water flows from the outer reaches of the formation toward the well.

Pure thermal stimulation does not appear to be an effective dissociation method[7,8], but it can be effectively used in conjunction with depressurization for localized applications involving the destruction of secondary hydrate and/or ice that often develop in the vicinity of the well and have the potential to inhibit flow and production. Similarly, the use of inhibitors is not recommended because of serious practical limitations[7,8] that include (a) rapid reduction in effectiveness because of inhibitor dilution by the H_2O released from dissociation, (b) the high cost (and limited recovery potential) of chemical inhibitors, and (c) the potential permeability reduction by hali-te precipitation in salt-based applications.

Note that the present study focuses on gas production from Class 2 accumulations that are confined between a nearly impermeable overburden and underburden. Class 2 accumulations without such strata can have a disappointingly low gas production because flow through the boundaries limits the effectiveness of depressurization and leads to large production volumes of undesirable water[10]. While a confining underburden is highly desirable, a near-impermeable overbur-den is critically important to the feasibility of gas production from a Class 2 deposit because of the development of an upper dissociation interface at the top of the hydrate body (a feature typical of gas production from hydrates), leading to gas accumulation that is augmented by buoyancy-driven gas ascent to the top of the formation[7]. Lack of a confining overburden could lead to gas loss though the overburden and release at the ground surface.

Geological System Description and Numerical Representation

System geology and geometry. The geologic system in this study is similar to that in the Mallik deposit[5,14] (Mackenzie Delta, Northwest Territories, Canada), and is analogous to that discussed by *Moridis et al.*[6] in their analysis of production from a Class 1 deposit. The Class 2 PA deposit was confined by impermeable overburden and underburden, and involved a 15m-thick HBL (with a

base at z = -1150 m), underlain by a 15m-thick WZ.

The geometry and configuration of the system are shown in Figure 2. The thickness of both the overburden and the underburden (i.e., the no-flow but heat-exchanging bounda-ries) is 30 m, which earlier calculations[7,18] had indicated to be sufficient to allow accurate heat exchange with the hydrate deposit during a 30-yr long production period (i.e., the standard life cycle of a well). The well at the center of this cylindrical hydrate deposit (Figure 2) had a radius r_w = 0.1 m. A no-flow (of fluids and heat) boundary was applied at the reservoir radius r_{max} = 567.5 m. This corresponded to a well spacing of about 100 ha (= 250 acres), with the no-flow boundary provided by the presence of other wells on the same spacing pattern.

Properties and initial conditions. The hydraulic and thermal properties of the various geological media (the HBL, WZ, and the confining layers), as well as the initial conditions, are listed in Table 1. We determined the initial conditions in the reservoir by following the initialization process described by *Moridis and Reagan*.[7] The initial P distribution followed the hydrostatic pressure gradient, and the initial T distribution follows a geothermal gradient of about dT/dz = 0.03 K/m and that was consistent with observations at the Mallik site[5]. Slight variations of dT/dz along z were caused by the effects of the permafrost, and of the thermal conductivities of the geologic media and the phases in the pores. Because the bottom of the hydrate stability zone was assumed to occur slightly below the elevation of the HBL base (which corresponded to a known hydrostatic pressure), the hydrate base temperature T_B was determined as slightly lower than the equilibrium hydration temperature T_e at that location (see Table 1 and Figure 1).

Both the HBL and the WZ were assumed to have the same homogeneous and isotropic properties, with a porosity ϕ = 0.35 and an intrinsic permeability $k = 10^{-12}$ m^2 (= 1 darcy). Similarly, the overburden and underburden were assumed to have the same properties. The initial hydrate saturation and aqueous saturation were S_H = 0.7 and S_A = 0.7, respectively, were consistent with saturation levels encountered in permafrost deposits[19,20], and were assumed to be uniformly distributed in the HBL. The relative permeability relationship and the corresponding parameters are based on data from the first field test of gas production from hydrates at the Mallik site[5], while the capillary pressure relationships and parameters are consistent with the ϕ and k of the HBL formation.

The numerical simulation code. The numerical studies in this paper were conducted using the TOUGH+HYDRATE simulator[17]. This code can model the non-isothermal hydration reaction, phase behavior, and flow of fluids and heat under conditions typical of natural CH_4-hydrate deposits in complex geologic media. It includes both an equilibrium and a kinetic model[21,22] of hydrate formation and dissociation. The model accounts for heat and up to four mass components (i.e., water, CH_4, hydrate, and water-soluble inhibitors such as salts or alcohols) that are partitioned among four possible phases: gas, aqueous liquid, ice, and hydrate. A total of 15 states (phase combinations) can be described by the code, which can handle any combination of hydrate dissociation mechanisms and can describe the phase changes and steep solution surfaces that are typical of hydrate problems.

Domain discretization. The cylindrical domain was discretized into 100 x 100 = 10,000 gridblocks in (r,z), of which 9,700 were active (the remaining being boundary cells). The uppermost and lowermost layers corresponded to constant T, no-flow boundaries, while the layers corresponding to the top and bottom confining layers (formations U and L, see Table 1) were impermeable but allowed heat exchange with the HBL and the WZ. To describe accurately the processes and phenomena occurring in the vicinity of the wellbore (which has been shown to be critically important to produc-tion[7,8]), we used a very fine discretization along the r direction (especially in the r < 20 m zone).

The HBL was subdivided into segments of uniform Δz = 0.25 m each along the z-direction. Such a fine discretization of is important (and possibly necessary) for accurate predictions[6,7], but a coarser discretization along the z axis is possible in the WZ[7]. This high definition provided the level of detail needed near the wellbore and in the entire hydrate-bearing zone. Assuming an equilibrium reaction of hydrate dissociation[23], the grid resulted in 29,100 coupled equations that were solved simultaneously.

The numerical simulations involved a physical representa-tion of the wellbore that was based on the approximation of wellbore flow by a process of Darcian flow through a pseudo-porous medium describing the interior of the well[7]. This pseudo-porous medium had a ϕ = 1, a very high $k = 10^{-9}$ - 10^{-8} m^2 (= 1,000 - 10,000 darcies), a capillary pressure P_c = 0, a relative permeability that was a linear function of the phase saturations in the wellbore, and a low (but non-zero) irreducible gas saturation S_{irG} = 0.005 (necessary to allow the emergence of a free gas phase in the well).

Simulation process and outputs. The maximum simulation period was the typical 30-year life span of the well, but the deposit was invariably exhausted much earlier. In the course of the simulation, the following conditions and parameters were monitored: Spatial distributions of P, T, and gas and hydrate phase saturations (S_G and S_H); Volumetric rate of CH_4 released from dissociation and of CH_4 production at the well (Q_R and Q_P, respectively); Cumulative volume of CH_4 released from dissociation and of CH_4 produced at the well (V_R and V_P, respectively); water mass production rate at the well (Q_W) and cumulative mass of produced water (M_W).

Well Design and Production-Related Processes

Evolution of production rate. We investigated the production performance of three different well designs described by *Moridis and Reagan*[7]. These designs involved different production intervals and operational procedures. In all cases, the initial mass rate of fluid production from the well was Q_{M0} = 9.2 kg/s (= 5,000 BPD of water). This was half the Q_{M0} applied to the wells in the study of production from deeper, warmer oceanic Class 2 deposits[7].

The initial stages of production invariably involved fluid removal (practically 100% water) almost exclusively from the WZ because of the very low k_{eff} of the HBL. Continuous fluid withdrawal from the WZ leads to the evolution of a dissociation interface along the HBL base because of the very low compressibility of water (which allows the depressuri-zation disturbance to be sensed over a large area along the HBL base) and the low k_{eff} of the hydrate interval (which promotes horizontal flow along the HBL base). As dissociation proceeds and the hydrate recedes along the HBL base, the hydrate interface advances upward[7]. A unique feature of gas production from hydrates (universal to all hydrate deposits) is the development of another horizontal dissociation interface that develops at the top of the hydrate interval and advances downward during depressurization-induced dissociation[6,7]. This is caused by the combination of depressurization (which leads to dissociation-induced cooling) and the resulting early reversal of the geothermal gradient at the upper reaches of the HBL (leading to heat flow from the overburden into the HBL and reversing its initial direction).

As in the case of an oceanic Class 2 deposit of *Moridis and Reagan*[7], a mass production rate Q_M was imposed at the well, and the production rates of the aqueous and gas phases were monitored. Gas emerged at the well after S_G in the reservoir exceeded the irreducible level S_{irG}. An important feature of depressurization-based gas production from hydrates is that the total mass rate Q_M of produced fluids (gas and aqueous phases) cannot be maintained constant, but needs to decrease as time advances[7,8]. This is a consequence of the continuously increasing contribution of gas to the production stream for any given Q_M, with a corresponding decrease in the water production. As more low-density gas replaces the denser water in the production stream, a point is reached where the system effective permeability is incapable of supplying the well with the prescribed Q_M, resulting in *cavitation* at the well (characterized by rapid pressure drops, which, if left unchecked, can reach levels below the atmospheric). This necessitates a reduction in Q_M if production is to continue.

Note that a reduction in Q_M does not necessarily lead to a decline in the rate of CH_4 production Q_P. While such a decline is expected immediately after the Q_M reduction, Q_P can match (and exceed) the earlier rate as the increasing gas contribution compensates for the reduction in total mass production. However, an eventual decline in Q_P is inevitable because of the monotonically declining T as dissociation proceeds. The cooling is caused by the endothermic nature of dissociation (which absorbs heat from its environment to fuel the reaction), in addition to the Joule-Thompson effect, and is in competition with the continuing pressure drop in the deposit. While initially the pressure drop (which enhances dissociation) outweighs the adverse offects of lower T (which slows dissociation), eventually the rate of Q_R slows significantly, resulting in a decline in Q_P.

Secondary hydrate can often form next to the wellbore after the destruction of the primary (original) hydrate at that location. This is possible if P at that location remains relatively high (above the quadruple point, see Figure 1), while T drops below the hydration temperature T_e. In addition to the unavoidable dissociation-induced cooling, the Joule-Thompson effect is at its maximum in the immediate vicinity of the well, where the highest gas flow velocities occur. If dissociation is very rapid or gas velocities are very high, ice can also form, especially when S_H is high and/or T is already low. Secondary hydrate and ice can accumulate next to the well at saturations sufficiently high to severely restrict ("choke") flow to the well, leading to cavitation. In this case, hot water injection can be used to destroy these solid phases and restore production.

Case A: Short production interval (Base case). The base case involves a production (perforated) interval that begins at the HBL base and extends 5m into the WZ. The decision to locate the perforated interval into the WZ below the hydrate zone is based on the very low permeability in the HBL (caused by the high $S_H = 0.70$, see Table 1) and the need to ensure a sufficiently high Q_M at the well. This is the simplest possible design, involves conventional technology, and poses no particular technical challenges.

Case B: Long production interval. In Case B, the production interval is unheated, covers the entire thickness of the HBL, and extends an additional 5 m into the WZ. This simple design involves conventional technology, and is initially equivalent to that in Case A. However, the active production interval becomes progressively larger and k_{eff} in the HBL next to the well increases as hydrate dissociation advances. Thus, this well design promotes the evolution of a cylindrical interface of hydrate dissociation around the well in addition to the horizontal dissociation interface at the bottom of the hydrate interval (which advances upward). Other significant advantages of the well configuration in Case B include the access it provides to the upper dissociating interface (and the gas that accumulates at this location), and the ability of the system to automatically allocate and seamlessly shift production to the most favorable part of the well, as dictated by phase mobilities and thermodynamics. This is important if secondary hydrate and/or ice are formed near the well.

For a given Q_M, the significantly larger production interval, coupled with the expanded area of dissociation, was expected to result in correspondingly milder pressure drops and a lower gas velocity (after gas emerges) in the vicinity of the well. This was in turn expected to lead to a reduction in the rate of cooling around the wellbore because of (a) the reduced rate of the endothermic dissociation reaction (caused by the milder pressure drop) and (b) the lessening of Joule-Thompson cooling (a consequence of the lower gas velocities). There was an expectation that higher T could delay, slow, and/or possibly prevent the formation of secondary hydrate around the well, and also prolong the production time between cavitations.

However, the analysis of production from marine Class 2 deposits yielded results that were not consistent with these expectations because rapid secondary hydrate formation caused well choking that did not allow long-term production[7]. Although this appears counterintuitive, it has a rational basis: it is attributed to the release of large amounts of gas by the rapidly dissociating warm oceanic hydrates (about 7 K warmer than the permafrost deposit in the current study), and the corresponding relatively rapid cooling. The combination of large amounts of gas with low T in the vicinity of the wellbore lead to the rapid hydrate reconstitution and flow blockage.

Case C: Variable production interval with outer wellbore heating. Case C involves a well that is initially similar to the one in Case A (with the perforated interval extending 5 m into the WZ), from which it differs in that the outer wellbore surface is heated (Figure 3). This heating causes thermal dissociation of the hydrate next to the well and leads to the creation of a zone of high k_{eff} in the HBL and a cylindrical dissociation interface around the well. Electrical heating may be used (at least initially) if the S_H of the undisturbed HBL is sufficiently high to make flow difficult. Because of superior heat transfer performance, warm water injection (injected at the upper part of the wellbore) was used at later times during production from oceanic Class 2 deposits[7]. Electrical heating, augmented with localized water injection near the HBL base (where secondary hydrates are likely to reconstitute) may be a better option in PA hydrates because it does not burden the lower Q_M with a water injection that will inevitably affect adversely gas production (Figure 4).

The outer wellbore heating in this well design prevents the formation of secondary hydrate around the wellbore, and can provide a continuous flow pathway from both the cylindrical and the evolving upper horizontal dissociation interfaces to the perforated interval[7]. Such access is by no means guaranteed in the unheated Case B (in which it can be blocked by secondary hydrate formation), and very unlikely in Case A. The expectation is that fluid withdrawal using this well design will result in maximum gas release and production by maximizing the total dissociation area and access to the three interfaces (i.e., the cylindrical, the upper and the lower horizontal ones). As the cylindrical and the lower horizontal dissociation interfaces continue to recede during dissociation, it is possible to expand the production interval upward into the HBL (from its initial upper limit at the base of the hydrate zone) and reap the benefits of a longer perforated interval.

The well may be further modified at a later stage (usually when less than 40% of the original hydrate remains) when there is significant gas accumulation at the top of the reservoir. Despite high S_G and large volumes, this gas cannot be recovered by using a conventional well perforated at the top of the formation because, after an initial short, high-rate, production period (lasting from hours to weeks), the well is blocked by secondary hydrate and/ice. The problem is alleviated by modifying the well according to the design of Figure 5, which involves alternating thin zones (about 1 m) of gas production and warm water injection. The warm water is injected at a low rate (< 1 kg/s) at a relatively low T (the reservoir is already cold because this well configuration is applicable only to an advanced stage of dissociation), and either prevents the formation of secondary hydrate or ice through mixing with the incoming fluid stream, or destroys pre-existing hydrate and ice blockages by thermal stimulation.

System Response During Production in Case A

Gas and water production. Figure 6 shows the evolution of Q_R, Q_P, and of the average production rate $Q_{avg} = V_P/t$ in the base Case A. Figure 7 shows the corresponding Q_W and M_W, in addition to the Q_M imposed at the well.

Q_R increases rapidly as the depressurization disturbance propagates along the lower interface and induces dissociation (because of the near-incompressibility of water). A local maximum of Q_R = 1.15 ST m^3/s (about 3.5 MMSCFD) is reached very early, before a mild decline begins. This is attributed to the combination of a locally higher P (caused by gas accumulation in the deposit because the released gas cannot yet be produced at the well when $S_A < S_{irA}$) and the resulting lower T, both of which slow dissociation until more heat arrives from the boundaries and gas production begins in earnest. When this occurs at about t = 200 days, Q_R increases again rapidly, as gas production enhances depressurization and further dissociation. The increase is monotonic, and continues until the first cavitation event (which defines the first production cycle) occurs at t = 1020 days. At that time, Q_R = 1.78 ST m^3/s (= 5.43 MMSCFD) and Q_P = 1.50 ST m^3/s (= 4.78 MMSCFD). The gas production rate (as described by Q_P) is initially (when t < 200 days) very low, but then it begins to increase rapidly and monotonically. During the same period, Q_W declines continuously (Figure 7).

In the second production cycle, Q_M is reduced (Figure 7) for the reasons discussed earlier, and production resumes. As discussed in detail by *Moridis and Reagan*[7], the decrease in Q_M results in an initial reduction in Q_R, Q_P and Q_w (Figures 6 and 7). After the resumption of production, both Q_R and Q_P increase rapidly and monotonically, and reach levels that exceed their respective values at the end of the first production cycle when the second cavitation (marking the end of the second production cycle) occurs at t = 1,550 days. At that time, the maximum Q_R (= 1.98 ST m^3/s = 6.04 MMSCFD) and Q_P (= 1.95 ST m^3/s = 5.95 MMSCFD) levels are observed.

The third and fourth production cycles follow the same pattern: (a) the reduction in Q_M produces a corresponding initial reduction in reduction in Q_R, Q_P and Q_w, but (b) Q_R and Q_P continuously increase during each cycle, while (c) Q_w decreases (Figures 6 and 7). What is different from the first two cycles is that the maximum Q_R and Q_P at the end of each cycle follow a declining trend. This is caused by gas production exceeding gas release, i.e., $Q_P > Q_R$, for the reasons discussed earlier, with gas accumulated earlier in the researvoir supplying the balance.

The fifth production cycle is the longest, lasting from t = 2,400 days until t = 5,860 days. The most interesting feature of the cycle is a spike in gas production (Q_P) at about t = 4,300 days. It is caused by a drop in P below the quadruple point near the well, leading to the dissociation of a thin layer of hydrate near the well. The elimination of this blockage and the uninihibited gas access to the well (without any further secondary hydrate formation) are the reasons for this surge in Q_P. Q_R is practically constant during this cycle, exhibits only a mild increase after the Q_P spike, and drops to zero (indicating hydrate exhaustion) at t = 5,640 days.

Subsequent production cycles exhibit precipitous reductions in Q_R because the only gas source is the CH_4 stored in the reservoir during earlier dissociation. Production can stop at any point deemed uneconomical. A criterion for the determination of this point (in addition to the Q_P magnitude) may be the Q_{avg} magnitude and trend. Figure 6 indicates that Q_{avg} remains practically constant at 1.02 ST m^3/s (= 3.11 MMSCFD) from about t = 2,400 days until t = 5,860 days, and then begins to decline slowly.

Q_W is initially almost equal to Q_M, but represents a progressively diminishing portion of Q_M as time advances because of the increasing contribution of gas to the production stream until the depletion of the hydrate (Figure 7). Past that point, the water contribution to Q_M increases again.

Compared to production from oceanic Class 2 hydrate deposits[7], there is significant difference in the early Q_P response. Thus, the stage of monotonic and rapidly increasing gas production begins earlier (i.e., at about t = 60 days) in PA deposits, as opposed to the several hundred days needed in oceanic accumulations. The difference is due to the insignificant contribution of dissolved gas to production from PA deposits. Because of the lower P, the amount of dissolved gas is small, and gas release originates almost exclusively from gas dissociation. Conversely, the higher P in oceanic accumulations lead to large initial releases of dissolved gas that help maintain a high pressure, prevent effective dissociation, and result in low gas production for long times.

Figure 8 shows the V_R and V_P in the base Case A. At the end of the simulation (t = 6,480 days), the hydrate has long been exhausted (as indicated by the flat portion of the V_R curve after t = 5,630 days), and, if geomechanical stability is not a consideration, a very high recovery ($V_P > 0.95\ V_R$) is feasible. During the 6,480 days of the simulation, a total of $V_P = 5.44\text{x}10^8$ ST m^3 (= $1.92\text{x}10^{10}$ ST ft^3) of CH_4 were produced.

Spatial distributions of S_H and S_G. The white lines in all of the figures that describe the spatial distribution of reservoir properties and conditions in Cases A through C denote the initial position of the base of the HBL, while the top of the HBL coincides with the z = –30 m datum. Comparison of the S_H to its initial distribution in the HBL provides a measure of the magnitude of dissociation of the hydrate.

Figures 9 and 10 show the evolution of the S_H and S_G distributions over time in the deposit near the wellbore (r < 20 m). As will be shown, the process of gas production from hydrate deposits is controlled by the phenomena that occur within a narrow radius near the well, hence the focus on this zone. Review of Figures 9 and 10 indicates that hydrate dissociation in Case A proceeds initially along the lower hydrate interface, and is more pronounced (as expected) close to the well. A cylindrical dissociation interface around the well is also evident. The entire hydrate zone appears to be dissociating even at an early stage (Figures 9b and beyond).

Secondary hydrates at saturations exceeding the original level (i.e., $S_H > 0.7$) are formed near the top of the perforated interval (where the gas velocities are highest and T is at its lowest), but their extent is limited and does not lead to structures that bock flow. Continuing depressurization and contact with warmer fluids arriving from the boundaries lead to the destruction of this secondary hydrate, which practically disappears after t = 1620 days. Elimination of the flow obstruction caused by the very thin secondary hydrate "skin" near the wellbore (Figure 9f) is responsible for the Q_P spike at about t = 4,300 days in Figure 6.

Figure 9 shows the evolution of the upper horizontal interface at the top of the HBL. As indicated earlier, this is a result of continuing depressurization and heat flows from the upper boundary. The upper dissociation interface is clearly shown in Figures 9b and beyond. The corresponding S_G distributions in Figure 10 indicate gas accumulation in the hydrate-free zone between the base of the overburden and the receding hydrate interface, leading to the highest S_G observed in the deposit. The reason for this accumulation is the continuing dissociation along the upper interface, in addition to the rising of the gas released elsewhere in the deposit due to buoyancy. The emergence of the upper dissociation interface and the gas accumulation at the top of the HBL have important implications for gas recovery, highlighting the necessity for overburden permeability barriers if gas production from hydrates is to become possible. Absence of such barriers will inevitably lead to gas escaping through the permeable overburden toward the ground surface. Advancing dissociation and gas release along the HBL base result in increasing S_G levels at that location (Figures 10b and beyond). However, S_G does not reach the levels at the top of the HBL because continuous flow to the well prevents gas accumulation.

Continuous production leads to the gradual dissociation of the entire hydrate body (Figures 9g and 9h), until the hydrate is exhausted (Figure 6). Of particular interest are the emergence of heterogeneous secondary hydrate structures near the well (Figures 9a to 9d) and the uniformity of the dissociation pattern of the hydrate along the reservoir radius (practically the same as that shown for r < 20 m in Figures 9f to 9h). Conversely, very different S_H and S_G distributions have been observed in gas production from oceanic Class 2 hydrates[7] when using the well configuration of Case A. These are characterized by isolation of the upper dissociation interface and impaired production[7]. The differences are attributed to the faster dissociation and larger gas availability in the warmer oceanic hydrates, which lead to the early (and substantial) formation of large secondary hydrates structures that cut off access to the upper dissociation interface.

Spatial distributions of T. The T distribution in Figure 11 indicates continuous cooling as dissociation and production proceed, and is consistent with expectations. Actually, it is possible to identify from Figure 11 regions of intense hydrate dissociation as the locations where significant T drops occur.

System Response During Production in Case B

Gas and water production. Figure 12 shows the evolution of Q_R, Q_P and Q_{avg} in Case B. Figure 13 shows the corresponding Q_W and M_W, in addition to the Q_M imposed at the well. The evolution of Q_R and Q_P is similar in patterns to those from Case A (Figure 6). We only have three production cycles. During each of the first two cycles, Q_R and Q_P increase rapidly monotonically, while the corresponding Q_w decreases continuously (Figure 13).

Unlike Case A, warm water injection is necessary to destroy the secondary hydrate accumulation around the wellbore at the end of the first two production periods. Thus, production in Case B proceeds in cycles, each of which has two stages: an initial long stage of continuous production, followed by cavitation, followed by a short stage of destruction of the secondary hydrate or ice blocking flow by injected warm water. The spike in Q_P at the beginning of the third production cycle occurs when the secondary hydrate

destruction provides access to the gas accumulated at the top of the formation. Q_R is initially roughly stable in the third cycle, until a jump at about t = 3,300 days caused by the P dropping below the quadruple point level. This leads to rapid dissociation of the remaining hydrate, until its exhaustion at t = 3,950 days. Q_w is initially constant in the third cycle, but begins to increase as the water released from dissociation reaches the well (Figure 13). Compared to Case A, the longer perforation interval allows exhaustion in a substantially shorter time (4,500 vs 6,480 days in Case A), leading to the Q_{avg} shown in Figure 12. At t = 3,950 days, Q_{avg}=1.46 ST m^3/s (= 4.44 MMSCFD), i.e., substantially higher than that in Case A. When Q_P consistently exceeds Q_R in the 2nd and 3rd cycle, gas production is partially fed by the gas stored in the reservoir during earlier dissociation.

There are fundamental differences between the performance of the well design in Case B during production from PA accumulations and from oceanic deposits[7]. Gas prodiction from oceanic deposits past a certain point is not even possible because of rapid formation of massive secondary hydrates that choke the well[7]. Conversely, production from PA deposits proceeds smoothly, and leads to practically full recovery of the resource (Figure 14). The results in Figures 12 and 13 appear to demonstrate the superiority of the long wellbore design in Case B over that in Case A during production from Class 2 PA deposits.

Figure 14 shows the evolution of V_R and V_P in Case B. At the end of the simulation (t = 4,500 days), the hydrate is exhausted (as indicated by the flat portion of the V_R curve after t = 3,900 days), and $V_P > 0.98V_R$ if production is not limited by geomechanical considerations. During the 4,500 days of the simulation, a total of $V_P = 5.56\text{x}10^8$ ST m^3 (= $1.96\text{x}10^{10}$ ST ft^3) of CH_4 were produced.

Spatial distributions of S_H and S_G. Figures 15 and 16 show the evolution of the S_H and S_G distributions over time near the wellbore (r < 20 m). As in all cases of gas hydrates[6,7,8], the process of gas production is controlled by the phenomena that occur within a short radius around the well, hence the focus on this narrow zone. The dissociation pattern is very different from that in Case A (Figures 9 and 10), but the features that are common to both cases are (a) the evolution of the upper dissociation interface and of a conical interface around the well, and (b) the gas accumulation between the receding upper hydrate interface and the base of the overburden.

Dissociation begins at both the lower interface at the HBL base and at the emerging upper interface at the base of the overburden, in addition to around the well (Figures 15a and 16a). These figures depict the easy flow of gas from the cone-shaped dissociation front and the upper interface to the perforated interval, which now spans the entire thickness of the HBL and extends 5 m into the WZ. This dissociation pattern is a direct consequence of the well design, which also leads to the evolution of secondary hydrate structures that encircles the well (Figure 15a) in a manner akin to a glove. This structure becomes thicker over time as hydrate accumulates on its outer surface. The finger-like appendix at the bottom of the structures appears to move away from the well as time advances because of hydrate dissociation along its inner surface (where depressurization is at its maximum) and accretion along its outer surface (where the temperature is low and free gas comes in contact with water. Destruction of the secondary hydrate structures requires less than 30 days and involves injection of 50 ^oC water (with a specific enthalpy of $H_W = 2.50\text{x}10^5$ J/kg) at a rate of Q_I = 1 kg/s.

Continuing dissociation along the upper interface and gas rise due to buoyancy lead to the creation of high-S_G gas bank above the main body of the hydrate, i.e., between the receding upper interface and the base of the overburden (Figure 16c and beyond). The implications of this pattern (universal to all hydrate classes under depresssurization-induced production) are significant, and have already been discussed. The S_H distribution in Figure 16h shows the significant destruction of hydrate during the 3240-day production period. The injection of warm ocean water can be easily seen in in Figures 16b, 16d and 16f, which show significantly-reduced S_G levels as the injected water expels the gas after destroying the secondary hydrate. Gas flow is easily restored when production resumes.

An interesting feature is the difference in appearance and location of the secondary hydrate barriers that develop during production: while barriers in Class 2 PA deposits are thick and are located immediately next to the wellbore, the barriers in oceanic deposits are thin, move away from the well, and are stabilized at a considerable distance[7].

Spatial distributions of T. The T distribution in Figure 17 indicates continuous cooling in the deposit as dissociation and production proceeds, and conforms to expectations. The effect of the barrier is obvious, indicating dissociation of the inner surface of the secondary hydrate structure (Figures 15a, 15c and 15e), in addition to Joule-Thompson cooling at the same locations. The presence of the injected warm water is evident in Figures 16b, 16d and 16f.

System Response During Production in Case C

Gas and water production. In Case C, electrical heat was initially applied to the outer surface of the wellbore at a rate of Q_Θ = 200 W/m (Figure 3). Figure 18 shows the evolution of Q_R, Q_P and Q_{avg}. Despite drastically different well designs, both Q_R and Q_P are remarkably similar in pattern and values to those from Cases B (Figure 12) during the first production cycle for the reasons explained earlier. An additional reason is that all three create roughly the same hydrate-free zone (and, consequently, a cylindrical or conical dissociation interface and a fast flow pathway) around the well, albeit by different means: Cases A and B by pure depressurization, while Case C by a combination of depressurization and thermal stimulation.

What is very different in Case C (as will be clearly shown later) is that secondary hydrate formation is minimal (to non-existent), and the several cavitation events that are evident at the end of each production cycle in Figure 18 (denoted by the subsequent drops in Q_P and Q_R, as dictated by the need to reduce Q_M) are not caused by flow obstruction by secondary hydrate formation but by the continuous replacement of the denser water by the lower-density gas in the production stream (see earlier discussion). Warm water was injected (at a rate Q_I = 1 kg/s and a $H_W = 2.75\text{x}10^5$ J/kg) at the bottom of the HBL to destroy the limited amount of secondary hydrate after the first cavitation event, but no more secondary hydrate was observed after that time. In all subsequent cavitation cases there was no need to inject hot water, and production resumed after reducing Q_M. The production cycles in Case C do not include a

warm water injection stage, but are only periods of continuous production punctuated by a simple Q_M reduction after each cavitation event.

After the first cavitation event, we increased the production interval by perforating an additional 2 m of wellbore into the HBL. This was possible because dissociation had turned the area around the wellbore at this location into a hydrate-free zone, and lead to an increase in Q_P. Beginning in the second production cycle, Q_P consistently exceeded Q_R, indicating that gas production was partially supported by the gas stored earlier in the reservoir.

Figure 19 shows Q_W and M_W, in addition to the Q_M imposed at the well. The patterns are analogous to those described in Case B, but the number of production cycles (and the corresponding reductions in Q_W) are larger than in Cases A and B. Q_W declines monotonically and consistently in every production cycle, as increasing amounts of gas reach the well. As Figure 20 shows, at the end of the 3850-day simulation period, a total of $V_P = 5.56\text{x}10^8$ ST m^3 (= $1.96\text{x}10^{10}$ ST ft^3) have been produced, i.e., the hydrate is totally exhausted and the CH_4 practically fully recovered. From Figure 18, the corresponding average gas production Q_{avg} = 1.66 ST m^3/s (= 5.06 MMSCFD), and is the highest of all three cases.

The results in Figures 26 to 29 demonstrate the clear superiority of the wellbore design in Case C over those in Cases A and B. Although the difference in performance between cases B and C is not very large, the avoidance of the evolution of possibly unpredictable hydrate barriers in close proximity to the well (Figure 16) during gas production represents a significant advantage. Note that case C is the only case of significant similarity of the well performance in PA and in oceanic deposits.

Spatial distributions of S_H and S_G. Figures 21 and 22 show the evolution of the S_H and S_G spatial distributions in the critical narrow zone (r < 20 m) around the wellbore. The dissociation pattern is different from that in Cases A (Figure 9) and B (Figure 15), but the universal features of hydrate dissociation persist. These include (a) the evolution of the upper dissociation interface and of a cylindrical interface around the well, and (b) the accumulation of gas above the receding upper hydrate interface under the overburden.

Dissociation begins at both the lower interface at the HBL base and at the cylindrical interface around the well, and then proceeds along the evolving upper dissociation interface (Figures 21 and 22). These figures confirm the intended objective of the design, i.e., to maintain easy access to the gas from all dissociation fronts to the well (Figures 3 to 5). The resulting dissociation pattern is a direct consequence of the well design. Its most important feature is the practical absence of secondary hydrates, which are formed only during the first production cycle (Figure 21b) and then never reappear. This is attributed to the continuous heating (initially electrical and later through warm water injection) along the outer surface of the wellbore. The S_H distribution in Figure 30h shows the significant destruction of hydrate as early as 1,916 days into the 3,850-day production period.

Figure 22 shows the accumulation of gas below the base of the overburden because of continuing dissociation and buoyancy-driven gas rise to the top of the formation. A significant gas bank is also observed below the hydrate body (Figures 22d and 22f). The injection of warm water can be easily deduced from the S_G distribution in Figure 22c (first production cycle). The location of the warm water injection next to the wellbore is identifiable as a low S_G region.

Of particular interest is the ice saturation S_I distribution in Figure 23. Ice evolves late, i.e., during the fourth production cycle, when the Q_M rate is sufficiently high to induce freezing and S_G is sufficiently high to avoid gas permeability limitations as the aqueous phase is replaced by an expanding solid ice phase. After the exhaustion of the hydrate at t = 3,380 days, the ice body shrinks because of continuous heat influx from the boundaries and the cessation of the dissociation.

Spatial distributions of T. The T distribution in Figure 24 clearly shows the continuous reservoir cooling expected during hydrate dissociation, as well as the effects of electrical heating and warm water injection. The flow of colder water released from dissociation to the well can be easily discerned.

Sensitivity Analysis

The sensitivity analysis focused on Case C because of the superiority of the corresponding well design. We investigated the sensitivity of gas production to the following conditions and parameters:

(a) The initial mass production rate Q_{M0},
(b) The initial hydrate saturation S_{H0},
(c) The stability of the hydrate deposit, as quantified by its temperature T and its deviation from the equilibrium temperature at the prevailing pressure,
(d) The intrinsic permeability k.

Sensitivity to Q_{M0}. Figure 25 shows the evolution of Q_R and Q_P when $Q_{M0} = 2\ Q_{M0,ref}$, where $Q_{M0,ref}$ is the Q_{M0} in the reference Case C. Comparison of Figures 26 and 18 indicates the maximum Q_P exceeds that in the reference Case C, the same V_P is produced over a significantly lower period, and, consequently, the corresponding Q_{avg} = 2.02 ST m^3/s (= 6.17 MMSCFD) is significantly higher. However, because of the inability to maintain a constant Q_M during the entire course of production, the increase in Q_{avg} is sublinear. The obvious conclusion is that gas production is favored by an increasing Q_{M0}., and the largest possible Q_{M0} should be applied initially.

Sensitivity to S_{H0}. Figure 26 shows the dependence of Q_P on S_{H0}. A lower S_{H0} leads to a lower Q_P because the higher initial k_{eff} (and, consequently, the faster depressurization and hydrate dissociation) are outweighted by the reduction in the resource. Thus, Q_P is

consistently lower (albeit slightly) when S_{H0} = 0.55 than in the reference case, in which S_{H0} = 0.7 (Table 1). This is the opposite to the response of deeper, warmer oceanic hydrates[7], in which Q_P increases with a decreasing S_{H0}.

Uniformity of system response away from the well. As previously indicated[7,8], processes and phenomena that occur within a narrow zone around the well control gas production from the entire hydrate deposit. This critical zone has a limited radius r_c (usually < 10-15 m), and fine discretization must be used for its simulation if these near-well phenomena are to be captured and accurately described. Dissociation and flow patterns are uniform and smooth for $r > r_c$. Figures 9, 15, 21 and 24 indicate that this is the case during production from Class 2 PA hydrates. This confirms the general observation that hydrate deposits under depressurization-induced production dissociate uniformly along the entire area of their horizontal interfaces, a behavior that is caused by the very large k_{eff} disparity between the HBL and its hydrate-free surroundings[7,8]. This dissociation pattern is quite different from that observed in gas production from Class 1 hydates.[6] The difference is attributed to the very different initial properties of the gas-rich Class 1 deposits (much lower thermal conductivity and larger specific heat, in addition to the substantial compressibility of the native gas phase), leading to faster cooling, localized processes and the emergence of substantially heterogeneous phase and property distributions.

Water-to-gas ratio. When technology and equipment availability do not pose challenges, the technical and economic feasibility of a production method is generally evaluated by employing two criteria: (a) an absolute criterion of sufficiently high Q_P, and (b) a relative criterion of an acceptably low water-to-gas ratio, defined as $R_{WGC} = M_W/V_P$. The continuously and rapidly declining R_{WGC} in Figure 27 confirms earlier observations[7,8] that this is a universal feature of depressurization-based production from hydrate deposits. The decline in R_{WGC} is reversed when the hydrate is exhausted. These observations are valid under any of the conditions and production methods investigated in this study. Hydrate deposits reserve their worst performance for the initial stages of production, but then they exhibit rapid and continuous improvement. This is in stark contrast to the production behavior in conventional gas reservoirs, in which R_{WGC} almost invariably increases over time.

The R_{WGC} of Case C in Figure 27 is lower than that of Case A and slightly so than that of case B, further indicating the superiority of the corresponding well configuration. The lower S_{H0} results in a more desirable (lower) R_{WGC} initially, although this later changes as the hydrate is exhausted. The general observation is that there are no glaring differences in the performance of these four cases in terms of water-to-gas ratio, as all of them have rather similar R_{WGC}. The case of $Q_{M0} = 2\ Q_{M0,ref}$ appears to be distinctivey different, as the corresponding R_{WGC} is consistently lower than that of the reference case during the entire course of production. This further underlines the desirability of a higher Q_{M0} as a production strategy. The shape and pattern of the R_{WGC} curves are entirely analogous to those observed in production from oceanic hydrate deposits[7], and appear to be characteristic of depressurization-based dissociation.

Summary and Conclusions

(1) We proposed three different well designs for gas production from Class 2 hydrate deposits in the permafrost. The first design (Case A) involves a production interval 5m long within the WZ (below the HBL). The production interval in the second design (Case B) is completed in the entire HBL and extends another 5m into the WZ. The third design (Case C) has the same configuration as Case A, but involves heating of the outer surface of the wellbore and may involve extensions of the production interval through additional perforations. All three designs involve conventional technology.

(2) We applied an initial mass withdrawal rate from the well Q_{M0} = 9.2 kg/s (= 5,000 BPD). In all cases, gas from dissociation is released rapidly into the hydrate deposit. Gas production is characterized by a relatively short (< 100 days) lead period of low gas production, followed by a period of rapid Q_P rise fueled by hydrate dissociation, and begins in earnest when S_G exceeds the S_{irG} level.

(3) Q_R and Q_P continue to increase until cavitation (characterized by rapid pressure drop at the well) occurs. The main reason for its occurrence is either the creation of a secondary hydrate structure (barrier) that blocks flow, or the replacement of the denser water by the lighter gas in the production stream at levels that cannot satisfy the imposed Q_M. Cavitation is treated by destroying the secondary gas hydrate barrier (if such a structure has formed during production) through warm water injection, and by reducing Q_M. A reduction in Q_M does not necessarily translate into a reduction of Q_P.

(4) Production proceeds in cycles between cavitation events. The first stage of each cycle involves continuous gas production and is several hundred days long. The second stage is short (a few weeks if hydrate destruction is needed), but may be very short (a few minutes) if only a reduction in Q_M is needed to overcome cavitation. Q_P continuously increases during the production stage of each cycle, with a corresponding reduction in Q_W.

(5) The results indicate that gas can be produced from hydrates at high rates using any of the three well designs when the HBL is bound by confining boundaries. Dissociation is characterized by features that are common to all deposits: (a) the evolution of an upper dissociation interface at the top of the hydrate layer (caused by heat flows from the upper boundary) in addition to the lower dissociation interface at the bottom of the HBL, and (b) gas accumulation below the base of the overburden because of continuing dissociation and buoyancy-driven gas rise to the top of the formation.

(6) Processes and phenomena that occur within a narrow zone around the well control gas production from the entire hydrate deposit. This critical zone has a radius r_c < 10-15 m, and fine discretization must be used in its simulations if these near-well phenomena are to be accurately described. Dissociation and flow patterns are uniform and smooth along the entire area of the horizontal interfaces for $r > r_c$.

(7) In the base Case A, the CH_4 production rate Q_P reaches a maximum level of 1.98 ST m^3/s (= 6.04 MMSCFD). During the 5,860 days of the simulation, a total of V_P = 5.44x10^8 ST m^3 (= 1.92x10^{10} ST ft^3) of CH_4 were produced at an average rate Q_{avg} = 1.02 ST m^3/s (= 3.11 MMSCFD).

(8) In Case B, during the 4,500-day production period, a total of V_P = 5.56x10^8 ST m^3 (= 1.96x10^{10} ST ft^3) of CH_4 were produced at an average rate Q_{avg} = 1.46 ST m^3/s (= 4.44 MMSCFD),. The well design in Case B allows access to upper dissociation interface and leads to the creation of a vertical dissociation interface around the well, but also leads to the creation of a secondary hydrate barrier around the well that needs to be destroyed regularly by water injection.

(9) In Case C, during the 3,850-day production period, a total of V_P = 5.56x10^8 ST m^3 (= 1.96x10^{10} ST ft^3) of CH_4 were produced at an average rate Q_{avg} = 1.66 ST m^3/s (= 5.06 MMSCFD). The well design in Case C allows access to upper dissociation interface, leads to the creation of a vertical dissociation interface around the well, and prevents the formation of secondary hydrate barriers around the well.

(10) The results of this study demonstrate the superiority of the wellbore design in Case C over those in Cases A and B in production under the permafrost conditions.

(11) Gas production increases with an increasing Q_M. Unlike the case of deeper, warmer oceanic hydrates[7], a decrease in S_{H0} does not lead to an increase in Q_P that would be expected because of the lower initial k_{eff}.

(12) Contrary to conventional gas reservoirs, R_{WGC} declines continuously and rapidly during depressurization-based production from hydrates, following a characteristic pattern and indicating a continuously improving performance. The R_{WGC} data confirm the superiority of the well design in Case C, and the desirability of applying the largest possible Q_{M0} for optimum production.

Nomenclature

Δr = Radial increment (m)
Δt = Timestep size (s)
Δz = Vertical discretization, i.e., in the z-direction (m)
C = specific heat (J/kg/K)
k = intrinsic permeability (m^2)
k_{eff} = effective permeability (m^2)
k_Θ = thermal conductivity (W/m/K)
$k_{\Theta RD}$ = thermal conductivity of dry porous medium (W/m/K)
$k_{\Theta RW}$ = thermal conductivity of fully saturated porous medium (W/m/K)
M_W = cumulative mass of water released into the ocean through the annular gravel pack (kg)
N_H = hydration number
P = pressure (Pa)
Q_Θ = rate of heat injection into the formation next to the well (W/m of wellbore)
Q_I = mass rate of injected warm water at the well (kg/s)
Q_M = mass rate of fluid withdrawal at the well (kg/s)
Q_P = volumetric rate of CH_4 production at the well (ST m^3/s)
Q_R = volumetric rate of CH_4 release from hydrate dissociation into the reservoir (ST m^3/s)
Q_W = mass rate of water release into the ocean through the annular gravel pack (kg/s)
Q_R = rate of CH_4 release from hydrate dissociation (ST m^3/s)
r,z = coordinates (m)
r_c = critical radius of maximum activity around the wellbore (m)
r_w = well radius (m)
r_{max} = maximum radius of the simulation domain (m)
R_{WGC} = cumulative water-to-gas ratio (kg/ST m^3)
S = phase saturation
t = time (days)
T = temperature (K or ^oC)
V_P = cumulative volume of CH_4 released into the ocean through the annular gravel pack (ST m^3)
V_R = cumulative volume of CH_4 released from hydrate dissociation (ST m^3)

Greek Symbols

λ = van Genuchten exponent – Table 1
ϕ = porosity

Subscripts and Superscripts

0 = denotes initial state
A = aqueous phase
e = equilibrium conditions
cap = capillary

G = gas phase
$G0$ = initial gas phase
H = solid hydrate phase
$H0$ = initial solid hydrate phase
irG = irreducible gas
irA = irreducible aqueous phase
n = permeability reduction exponent – Table 1
P = production stream
ref = reference Case C
R = rock

Acknowledgment

This work was supported by the Assistant Secretary for Fossil Energy, Office of Natural Gas and Petroleum Technology, through the National Energy Technology Laboratory, under the U.S. Department of Energy, Contract No. DE-AC02-05CH11231. The authors are indebted to Stefan Finsterle, John Apps and Dan Hawkes for their thorough review.

References

1. Sloan, E.D., *Clathrate Hydrates of Nautral Gases.* Marcel Decker, Inc., New York, NY (1998).
2. Milkov, A. V., "Global estimates of hydrate-bound gas in marine sediments: How much is really out there," *Earth Science Reviews* **66**(3), 183 (2004).
3. Klauda, J.B., Sandler, S.I., "Global distribution of methane hydrate in ocean sediment," *Energy & Fuels* **19**, 469 (2005).
4. Makogon, Y.F., "Gas hydrates: frozen energy," *Recherche* **18**(192), 1192 (1987).
5. Dallimore, S.R., Collett, T.S., Eds., "Scientific Results from the Mallik 2002 Gas Hydrate Production Research Well Program, Mackenzie Delta, Northwest Territories, Canada," *Geological Survey of Canada Bulletin* **585** (2005).
6. Moridis, G.J., Kowalsky, M.B., Pruess, K., "Depressurization-Induced Gas Pproduction From Class 1 Hydrate Deposits," *SPE Reservoir Evaluation & Engineering*, **10**(5), 458-481 (2007).
7. Moridis, G.J., Reagan, M.T., "Gas Production From Oceanic Class 2 Hydrate Accumulations," OTC 18866, 2007 Offshore Technology Conference, Houston, Texas, U.S.A., 30 April–3 May 2007.
8. Moridis, G.J., Reagan, M.T., "Strategies for Gas Production From Oceanic Class 3 Hydrate Accumulations," OTC 18865, 2007 Offshore Technology Conference, Houston, Texas, U.S.A., 30 April–3 May 2007.
9. Moridis, G.J., Sloan, E.D., "Gas Production Potential of Disperse Low-Saturation Hydrate Accumulations in Oceanic Sediments," *J. Energy Conversion & Management*, **48**(6), 1834-1849 (2007).
10. Kurihara, M., Funatsu, K., Ouchi, H., Masuda, Y., and Narita, H.: "Investigation of Applicability of Methane Hydrate Produ-ction Methods to Reservoirs With Diverse Characteristics", Paper 3003, in *Proceedings of the 5th International Conference on Gas Hydrates,* June 13–16, Trondheim, 714 (2005).
11. Hong, H., and Pooladi-Darvish, M.: "Simulation of Depressuri-zation for Gas Production from Gas Hydrate Reservoirs," *J. Can. Pet. Tech.*, **44**(11), 39 (2005).
12. Makogon, Y.F., *Hydrates of Hydrocarbons*. Penn Well Publishing Co. Tulsa, OK. (1997).
13. Wright, J.F., Dallimore, S.R., and Nixon, F.M.: "Influences of Grain Size and Salinity on Pressure-Temperature Thresholds for Methane Hydrate Stability in JAPEX/JNOC/GSC Mallik 2L-38 Gas Hydrate Research-Well Sediments", in Scientific Results from JAPEX/JNOC/GSC Mallik 2L-38 Gas Hydrate Research-Well, Mackenzie Delta, Northwest Territories, Canada. Dallimore, S.R., Uchida, T., and Collett, T.S., Eds., *Geological Survey of Canada Bulletin* **544**, 229 (1999).
14. Moridis, G.J., "Numerical Studies of Gas Production From Methane Hydrates," *SPE Journal*, **32**(8), 359 (2003).
15. Moridis, G.J., T. Collett, S. Dallimore, T. Satoh, S. Hancock and B. Weatherhill, "Numerical Studies Of Gas Production From Several Methane Hydrate Zones At The Mallik Site, Mackenzie Delta, Canada," *J. Petroleum Sci Eng.* **43**, 219 (2004).
16. Moridis, G.J., Seol, Y., Kneafsey, T., "Studies of Reaction Kinetics of Methane Hydrate Dissociation in Porous Media", (LBNL-57298) Proc. 5th International Conference on Gas Hydrates, Trondheim, Norway, June 13-16, 2005, Paper 1004, **1**, 21-30 (2005).
17. Moridis, G.J., Kowalsky, M.B., Pruess, K., "TOUGH-Fx/HYDRATE v1.0 User's Manual: A Code for the Simulation of System Behavior in Hydrate-Bearing Geologic Media," Report LBNL-58950, Lawrence Berkeley National Laboratory, Berkeley, CA (2005).
18. Moridis, G.J., Kowalsky, M.B., "Response of Oceanic Hydrate-Bearing Sediments to Thermal Stresses," *SPE Journal*, **12**(2), 253-268 (2007).
19. Dallimore, S.R., Uchida, T., and Collett, T.S. (eds.): "*Scientific Results from JAPEX/JNOC/GSC Mallik 2L-38 Gas Hydrate Research Well, Mackenzie Delta, Northwest Territories, Canada*", Geological Survey of Canada Bulletin **544** (1999).
20. Kurihara, M., Funatsu, K., Kusaka, K., Yasuda, M., Dallimore, S.R., Collett, T.S., and Hancock, S.H.: "Well-Test Analysis for Gas Hydrate Reservoirs: Examination of Parameters Suggested by Conventional Analysis for the JAPEX/JNOC/GSC et al. Mallik 5L-38 Gas Hydrate Production Test Results", in *Scientific Results from the Mallik 2002 Gas Hydrate Production Research Well Program, Mackenzie Delta, Northwest Territories, Canada*, S.R. Dallimore and T.S. Collett, eds., Geological Survey of Canada, Bulletin **585**, 1–31 (2005).
21. Kim, H.C., Bishnoi, P.R., Heidemann, R.A., and Rizvi, S.S.H.: "Kinetics of Methane Hydrate Decomposition", *Chem. Eng. Sci.*, **42**(7), 1645 (1987).
22. Clarke, M.A., and Bishnoi, P.R.: "Determination of the Intrinsic Rate of Methane Gas Hydrate Decomposition", *Chem. Eng. Sci.*, **55**, 4869 (2000).
23. Kowalsky, M.B., Moridis, G.J., "Comparison of Kinetic and Equilibrium Reaction Models in Simulating the Behavior of Gas Hydrates in Porous Media", (LBNL-60361) *J. Energy Conversion & Management*, **48**(6), 1850-1863 (2007).

Table 1 – Hydrate Deposit Properties

Parameter	Value
Water zone thickness	15 m
Hydrate zone thickness	15 m
Initial pressure P_B (at base of HBL)	1.067×10^7 Pa
Initial temperature T_B (at base of HBL)	286.65 K (13.5 ^oC)
Gas composition	100% CH_4
Initial saturations in the HBL	$S_H = 0.7$, $S_A = 0.3$
Intrinsic permeability $k_r=k_z$ (HBL and water zone)	10^{-12} m^2 (= 1 D)
Intrinsic permeability $k_r=k_z$ (overburden & underburden)	0 m^2 (= 0 D)
Grain density ρ_R (all formations)	2750 kg/m^3
Initial mass production rate Q_{M0}	9.2 kg/s (= 5,000 BPD)
Dry thermal conductivity $k_{\Theta RD}$ (all formations)	0.5 W/m/K
Wet thermal conductivity $k_{\Theta RW}$ (all formations)	3.1 W/m/K
Composite thermal conductivity model[16]	$k_{\Theta C} = k_{\Theta RD} + (S_A^{1/2}+S_H^{1/2})\ (k_{\Theta RW} - k_{\Theta RD}) + \phi\ S_I\ k_{\Theta I}$
Capillary pressure model[14,23]	$P_{cap} = -P_0\left[\left(S^*\right)^{-1/\lambda} - 1\right]^{-\lambda}$ $S^* = \frac{\left(S_A - S_{irA}\right)}{\left(S_{mxA} - S_{irA}\right)}$
S_{irA}	1
λ	0.45
P_0	2×10^3 Pa
Relative permeability Model[17]	$k_{rA} = (S_A^*)^n$ $k_{rG} = (S_G^*)^n$ $S_A^*=(S_A-S_{irA})/(1-S_{irA})$ $S_G^*=(S_G-S_{irG})/(1-S_{irA})$ EPM model
n (from Moridis et al.[6])	3.572
S_{irG}	0.02
S_{irA}	0.20

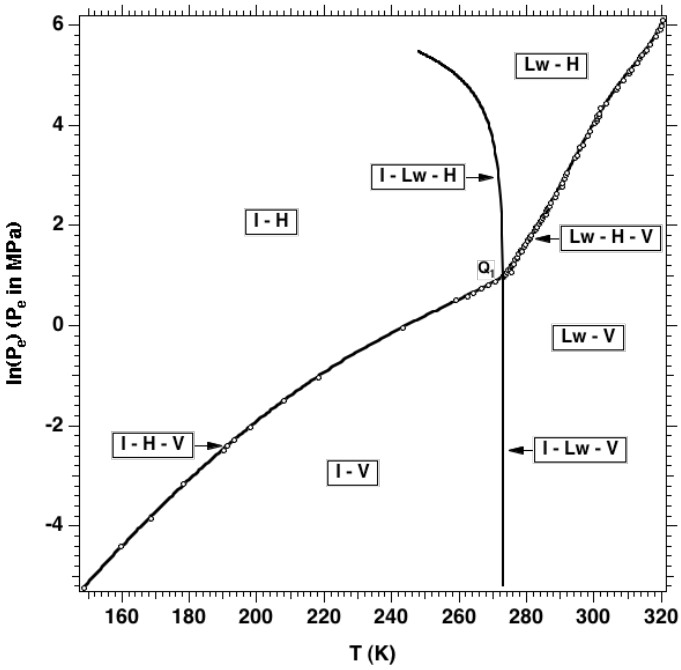

Figure 1 – Pressure-temperature equilibrium relationship in the phase diagram of the water–CH_4–hydrate system[17] (Lw: Liquid water; H: Hydrate; V: Vapor (gas phase); I: Ice; Q_1: Quadruple point = I + Lw + H + V)

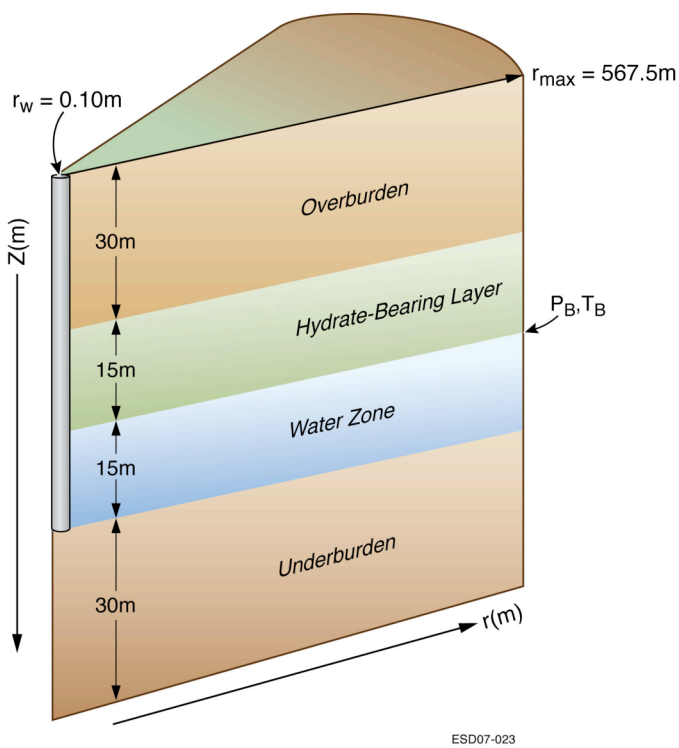

Figure 2 – A schematic of the permafrost Class 2 hydrate deposit simulated in this study.

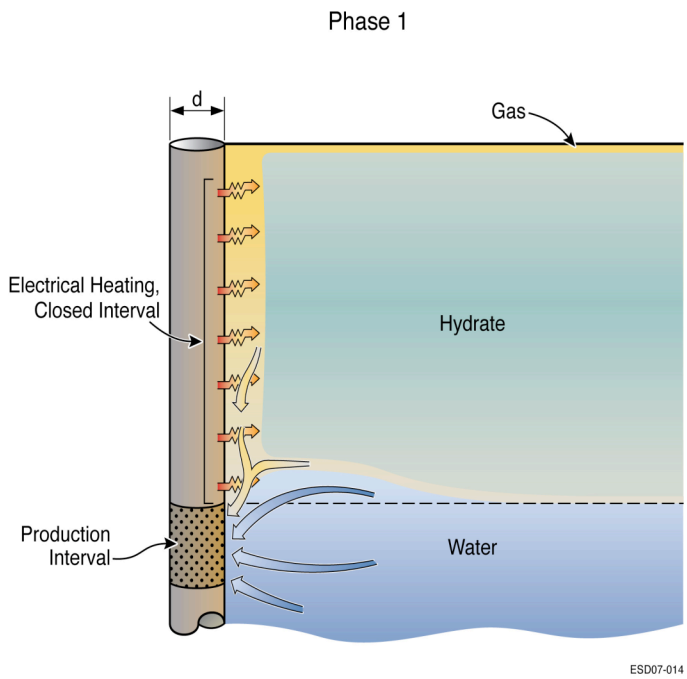

Figure 3 – Well design used in the initial production stages of Case C[7]. The production interval begins at the HBL and extends into the WZ, while the outer surface of of the wellbore in contact with the HBL is heated.

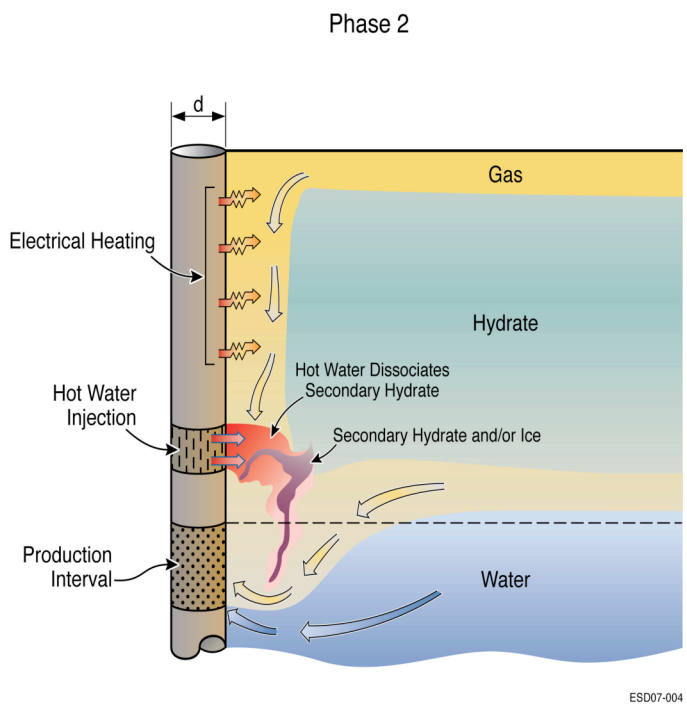

Figure 4 – Well design variant used in the early and intermediate production stages of Case C[7]. Warm water is injected into the formation near the top of the perforated interval.

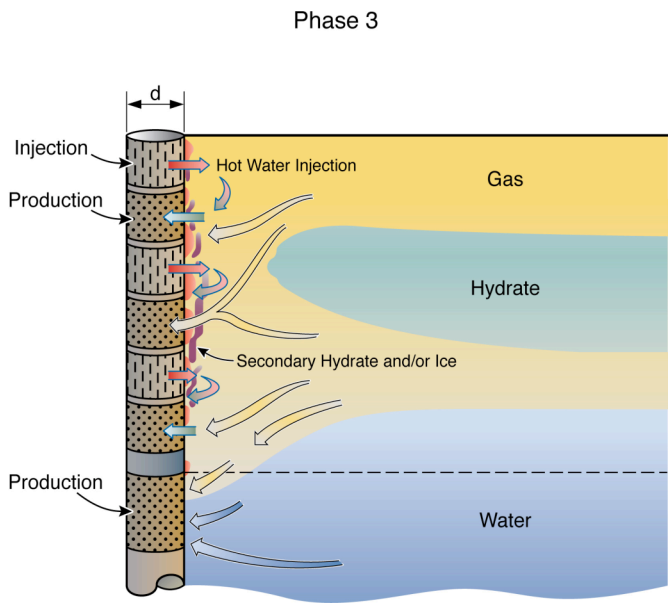

Figure 5 – Well design used in the late stages of production in Case C[7]. The system involves thin alternating zones of production and warm water injection.

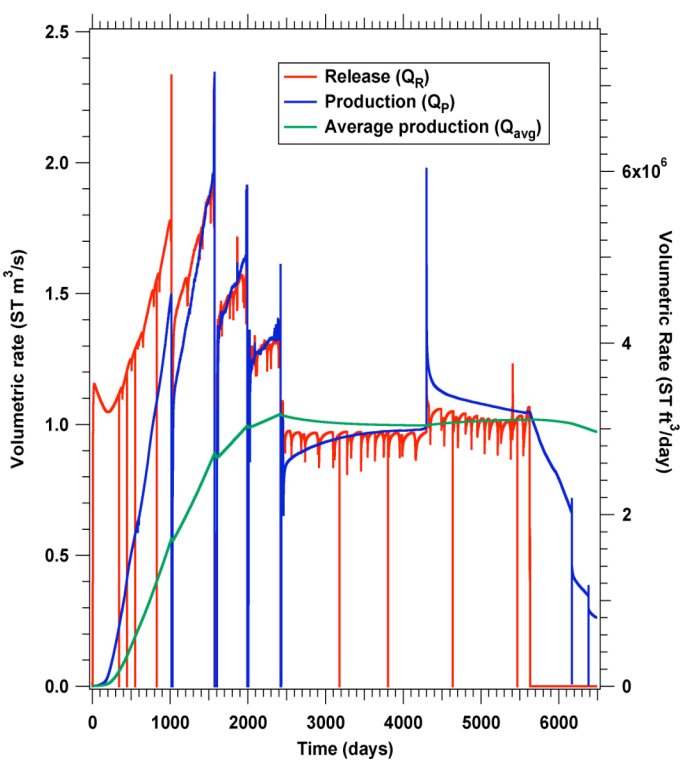

Figure 6 – Rates of (a) hydrate-originating CH_4 release in the reservoir (Q_R) and (b) CH_4 production at the well (Q_P) during production from the Class 2 PA hydrate deposit in Case A. The evolution of the average gas production rate (Q_{avg}) over the simulation period is also shown.

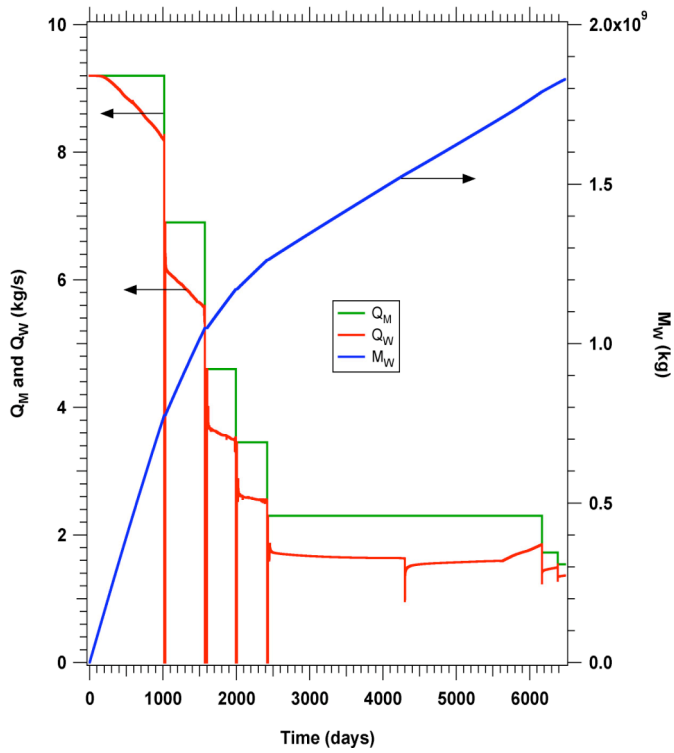

Figure 7 – (a) Mass rate of total fluid production, Q_M, (b) mass rate of H_2O production, Q_W and (b) cumulative mass of produced H_2O (M_W) during production from the Class 2 PA hydrate deposit in Case A.

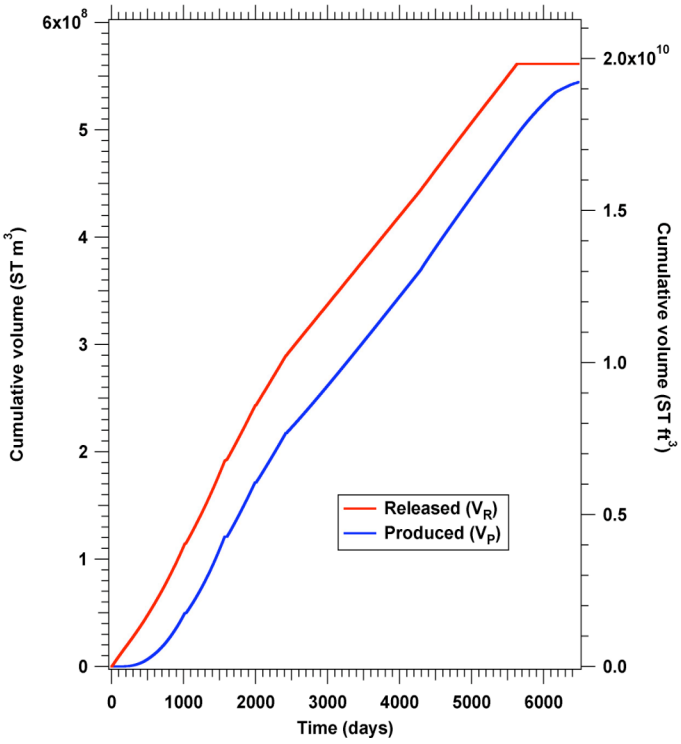

Figure 8 – Cumulative volumes of (a) hydrate-originating CH_4 released in the reservoir (V_R) and (b) produced CH_4 at the well (V_P) during production from the Class 2 PA hydrate deposit in Case A.

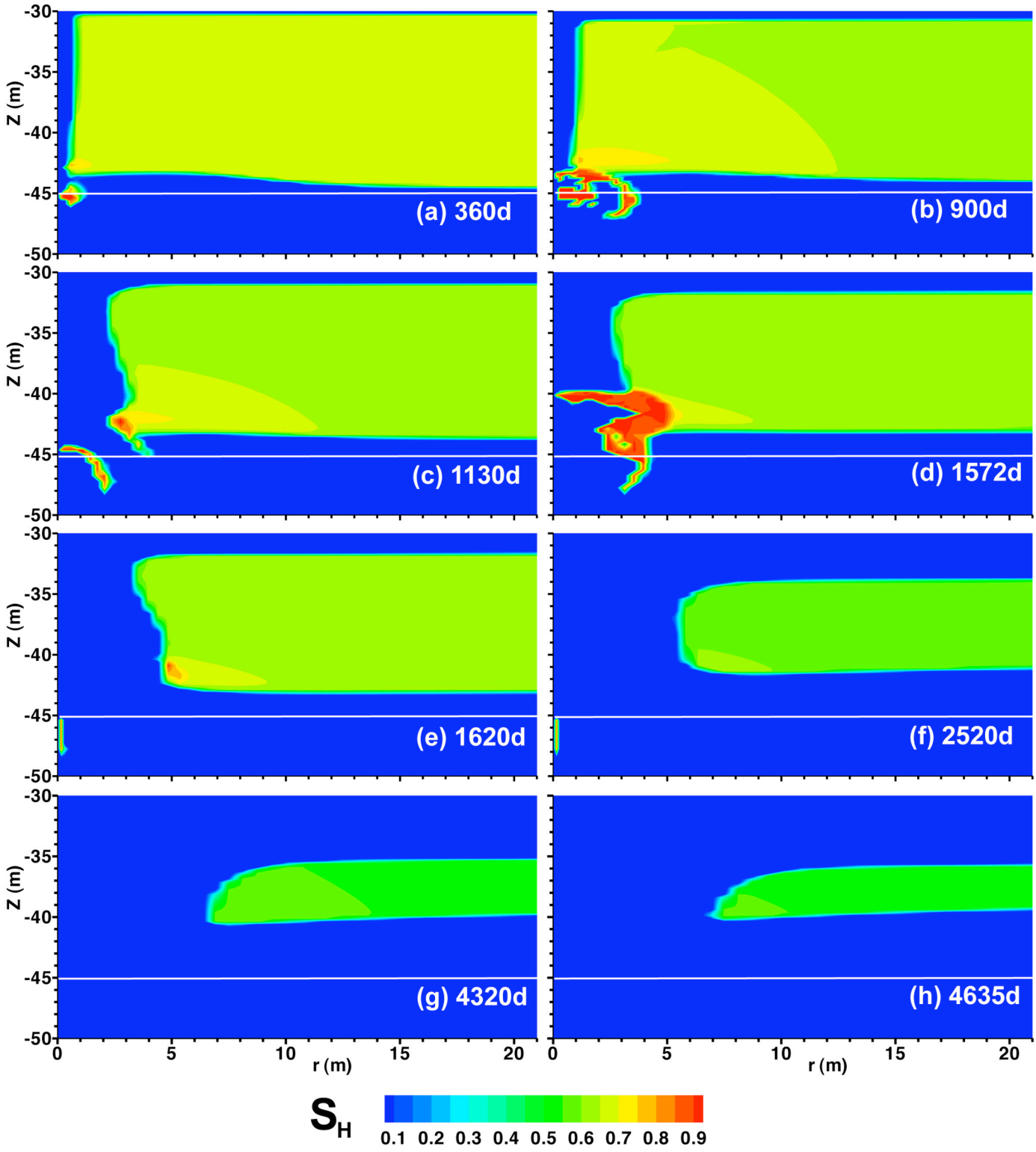

Figure 9 –Evolution of spatial distribution of S_H during gas production from the Class 2 PA hydrate deposit in Case A.

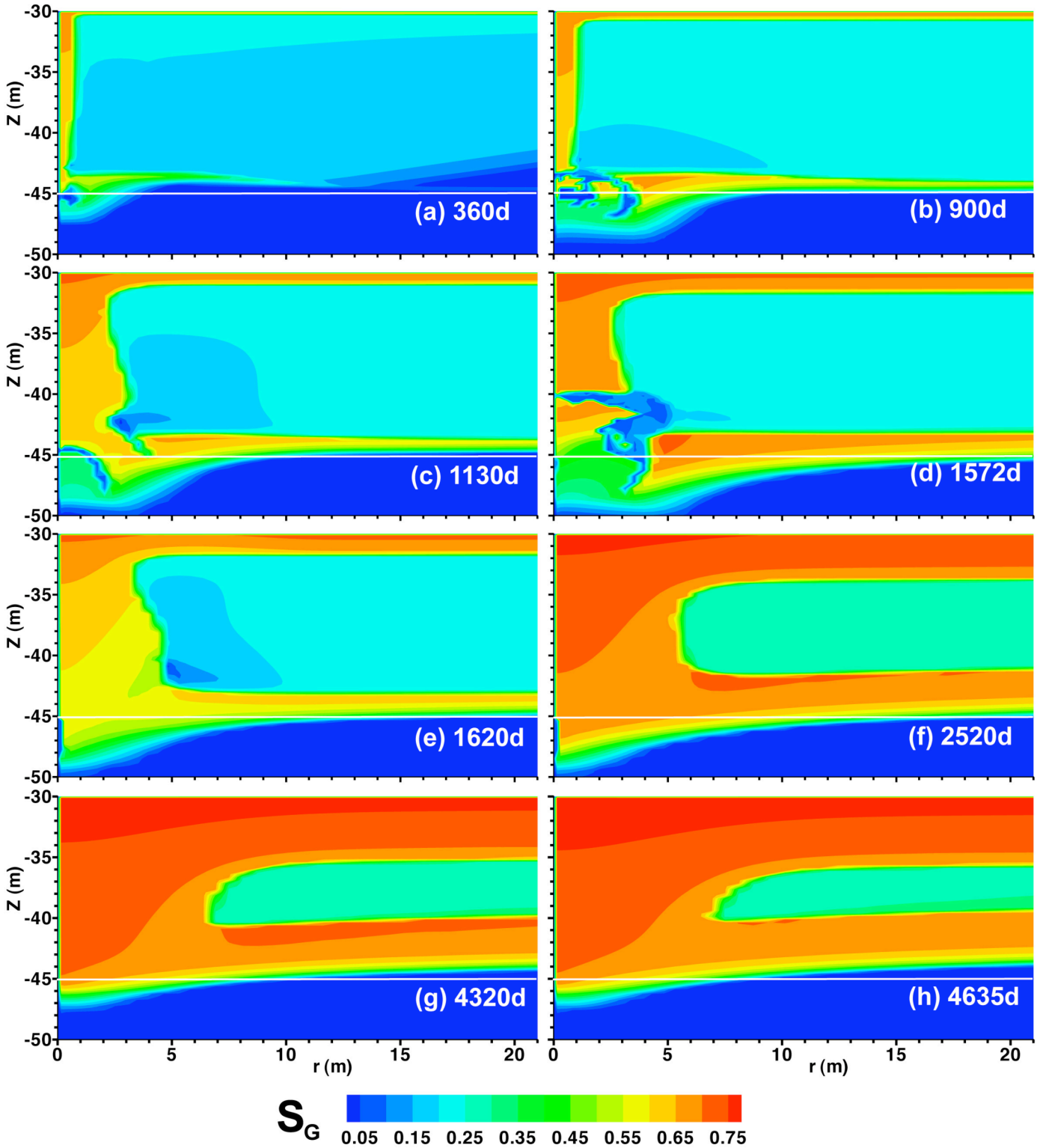

Figure 10 –Evolution of spatial distribution of S_G during gas production from the Class 2 PA hydrate deposit in Case A.

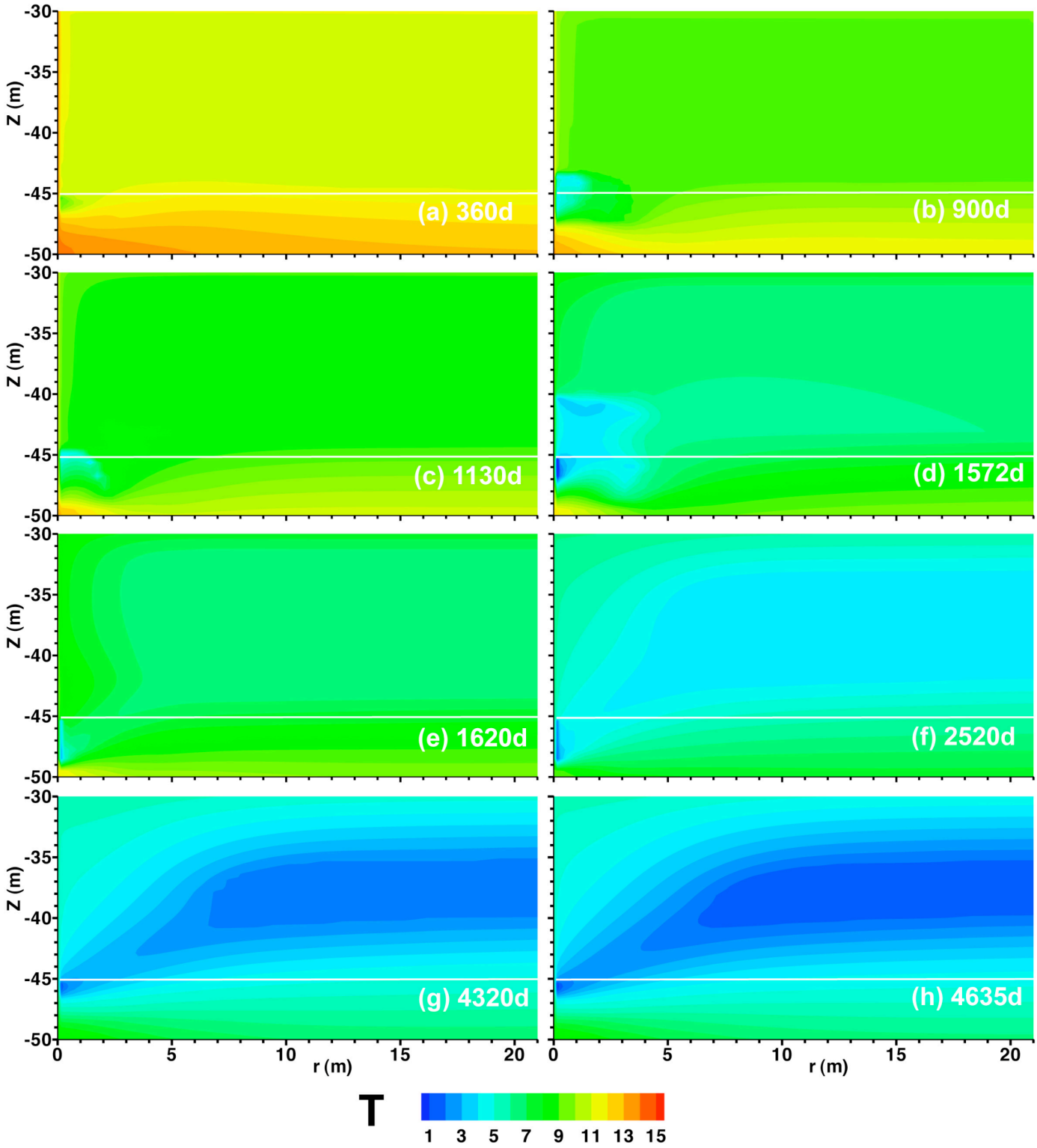

Figure 11 –Evolution of spatial distribution of T during gas production from the Class 2 PA hydrate deposit in Case A.

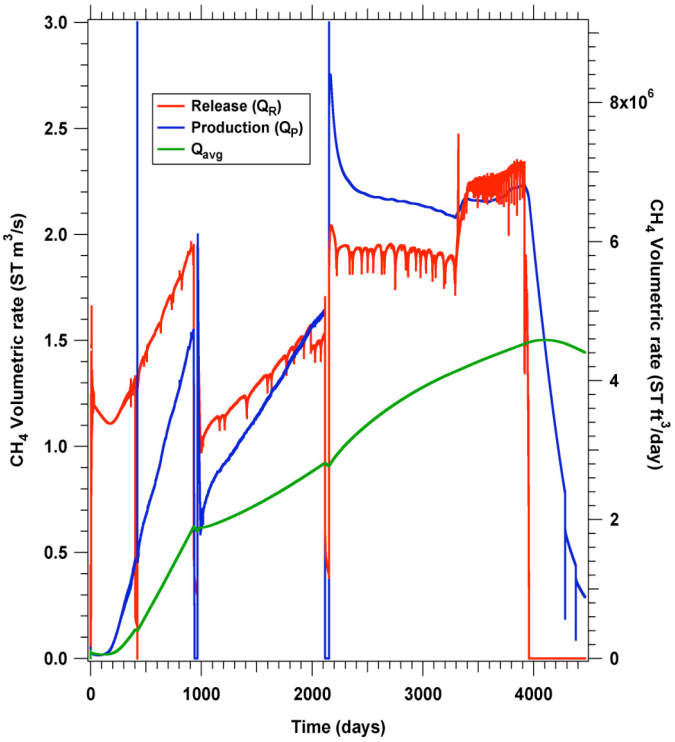

Figure 12 – Rates of (a) hydrate-originating CH_4 release in the reservoir (Q_R) and (b) CH_4 production at the well (Q_P) during production from the Class 2 PA hydrate deposit in Case B. The evolution of the average gas production rate (Q_{avg}) over the simulation period is also shown.

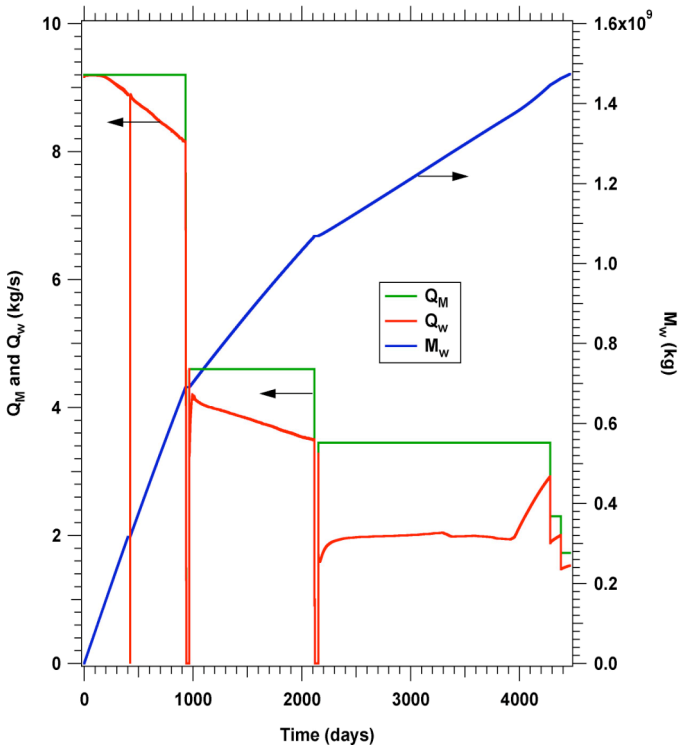

Figure 13 – (a) Mass rate of total fluid production, Q_M, (b) mass rate of H_2O production, Q_W and (b) cumulative mass of produced H_2O (M_W) during production from the Class 2 PA hydrate deposit in Case B.

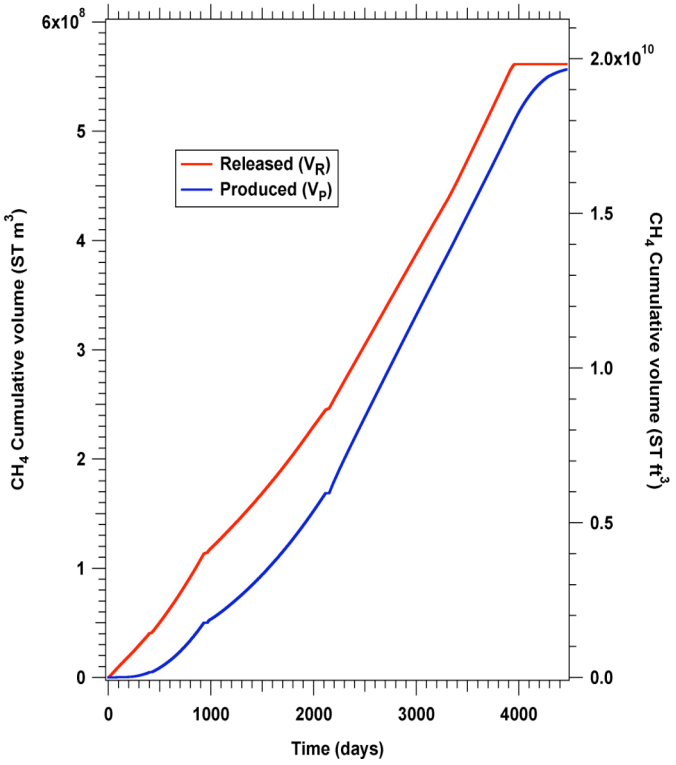

Figure 14 – Cumulative volumes of (a) hydrate-originating CH_4 released in the reservoir (V_R) and (b) produced CH_4 at the well (V_P) during production from the Class 2 PA hydrate deposit in Case A.

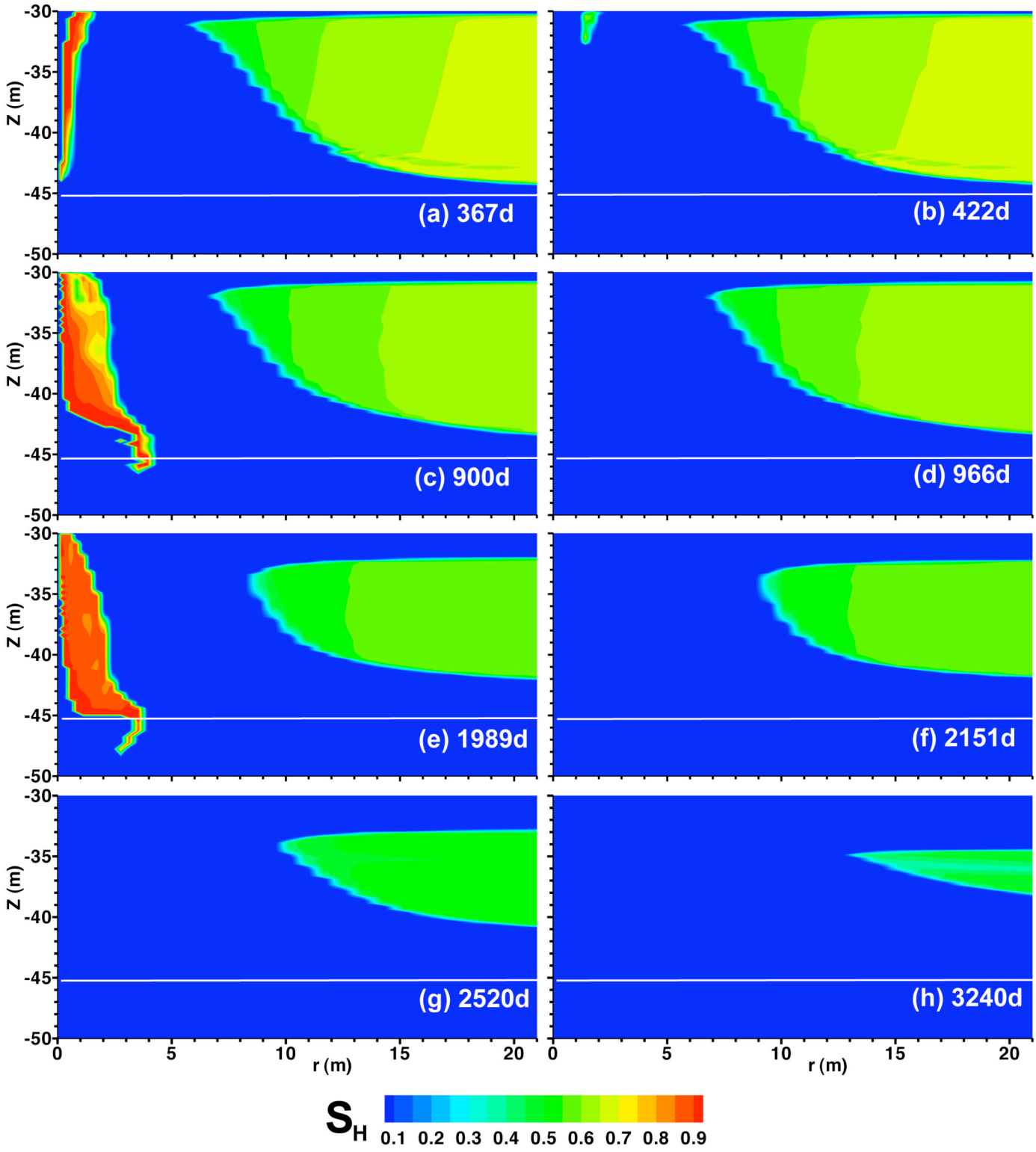

Figure 15 –Evolution of spatial distribution of S_H during gas production from the Class 2 PA hydrate deposit in Case B.

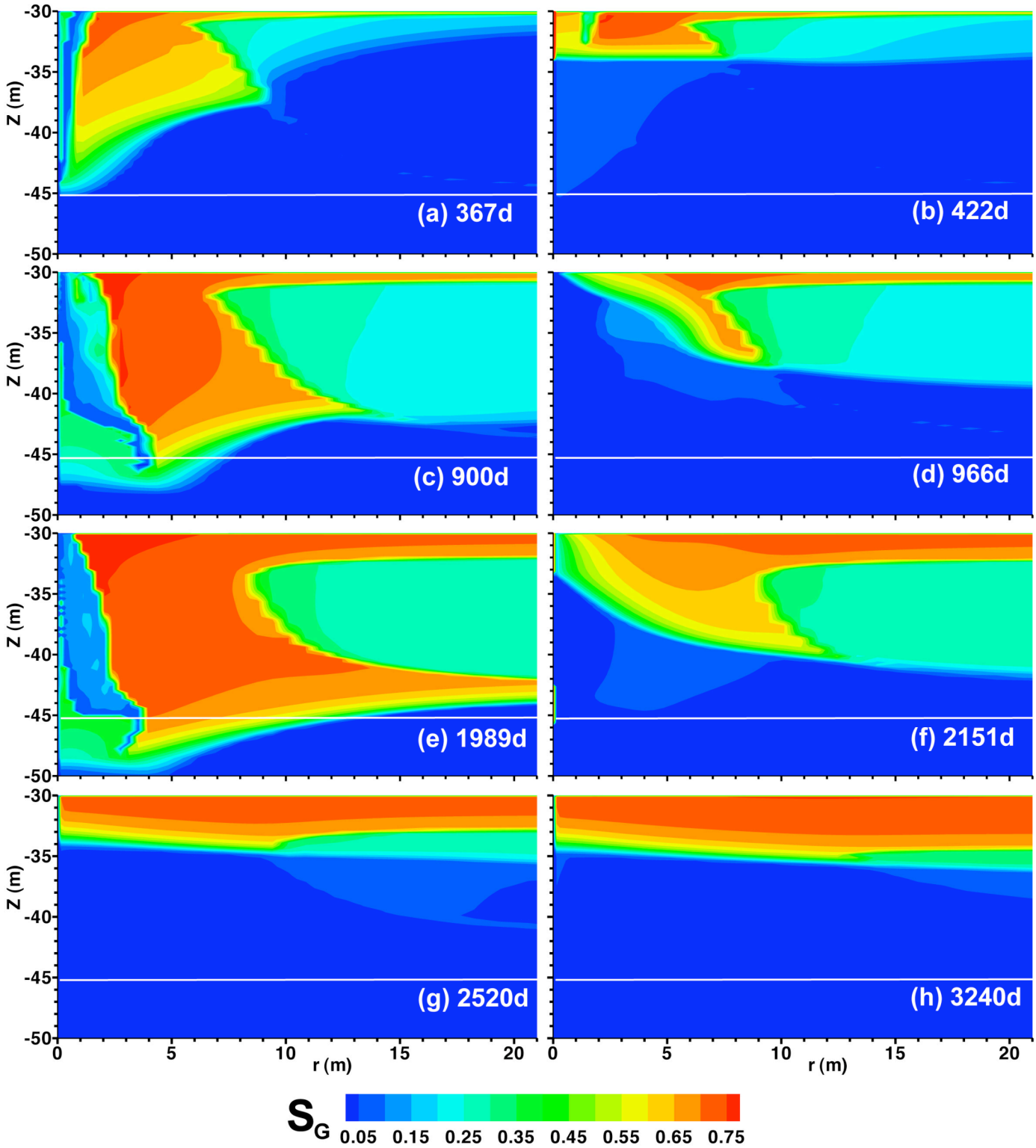

Figure 16 –Evolution of spatial distribution of S_G during gas production from the Class 2 PA hydrate deposit in Case B.

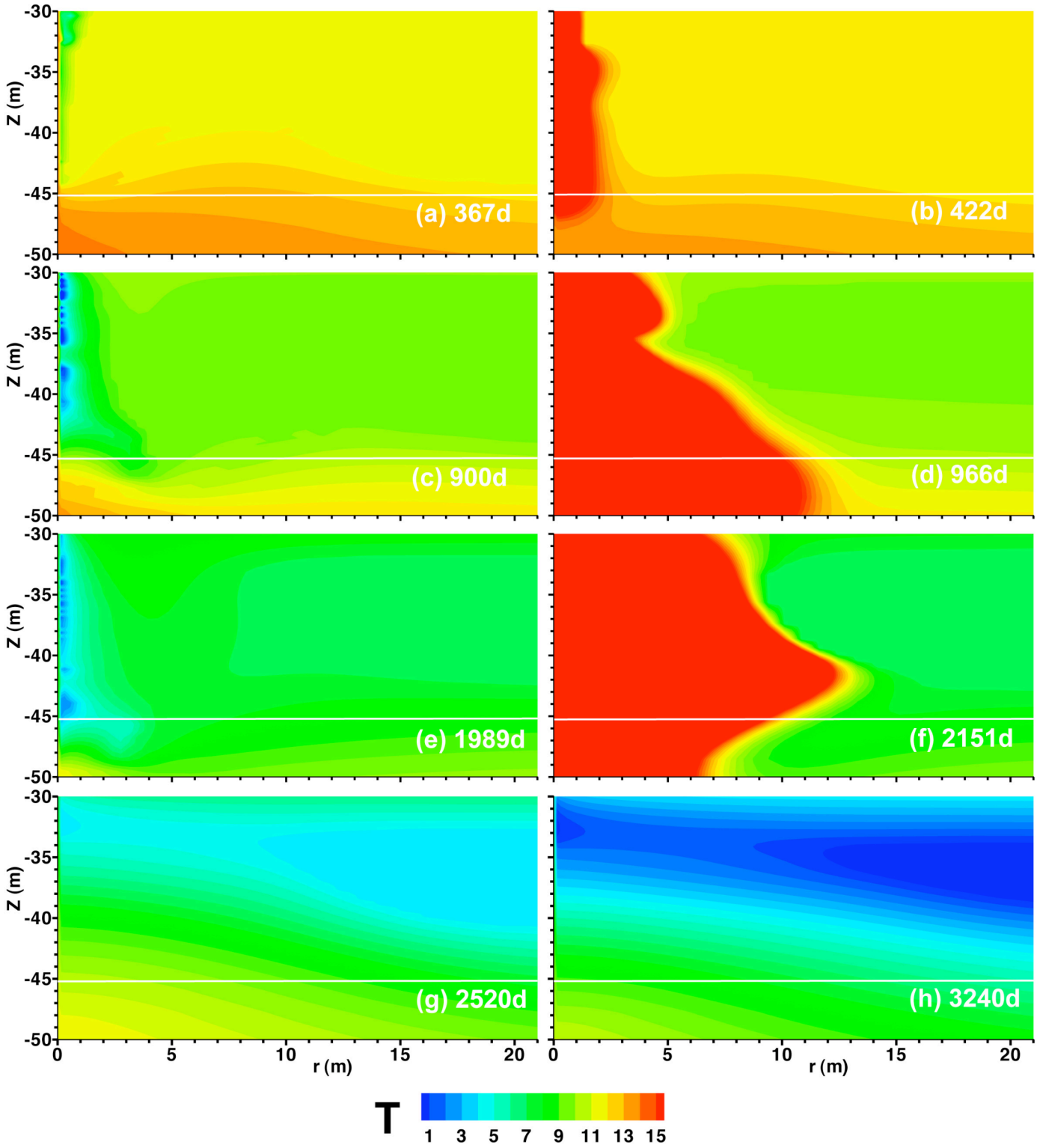

Figure 17 –Evolution of spatial distribution of T during gas production from the Class 2 PA hydrate deposit in Case B.

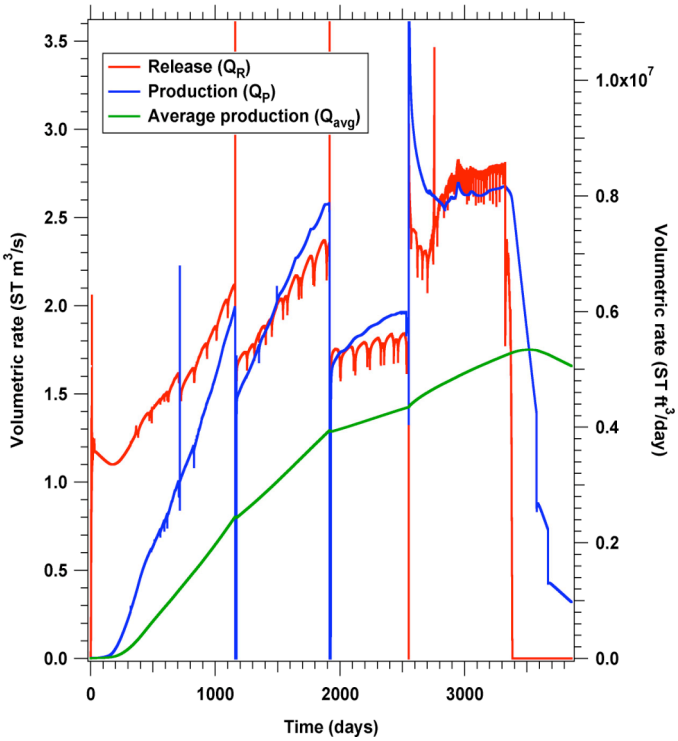

Figure 18 – Rates of (a) hydrate-originating CH_4 release in the reservoir (Q_R) and (b) CH_4 production at the well (Q_P) during production from the Class 2 PA hydrate deposit in Case C. The evolution of the average gas production rate (Q_{avg}) over the simulation period is also shown.

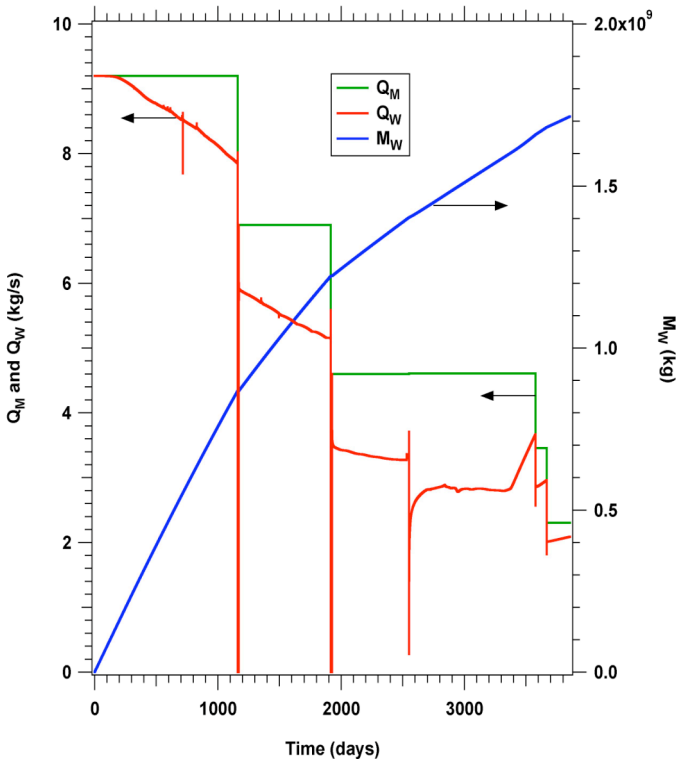

Figure 19 – (a) Mass rate of total fluid production, Q_M, (b) mass rate of H_2O production, Q_W and (b) cumulative mass of produced H_2O (M_W) during production from the Class 2 PA hydrate deposit in Case C.

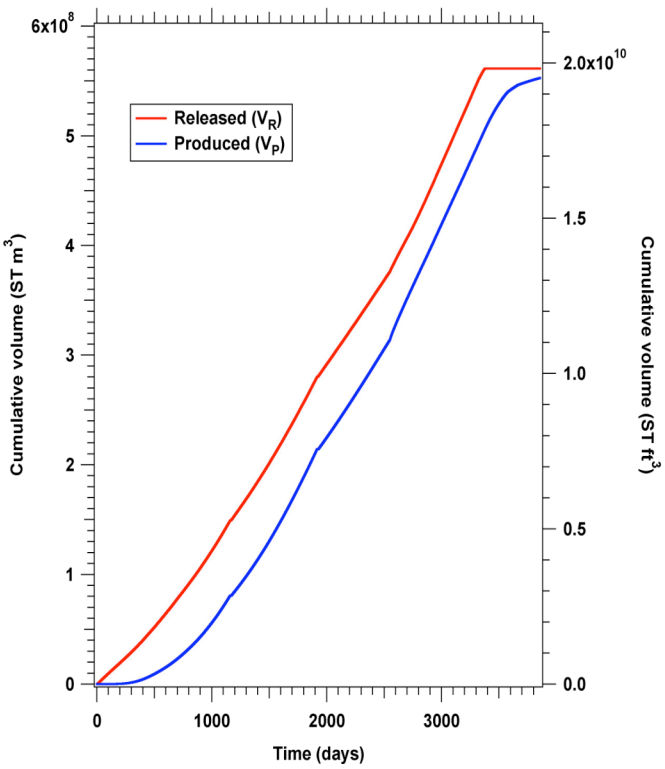

Figure 20 – Cumulative volumes of (a) hydrate-originating CH_4 released in the reservoir (V_R) and (b) produced CH_4 at the well (V_P) during production from the Class 2 PA hydrate deposit in Case A.

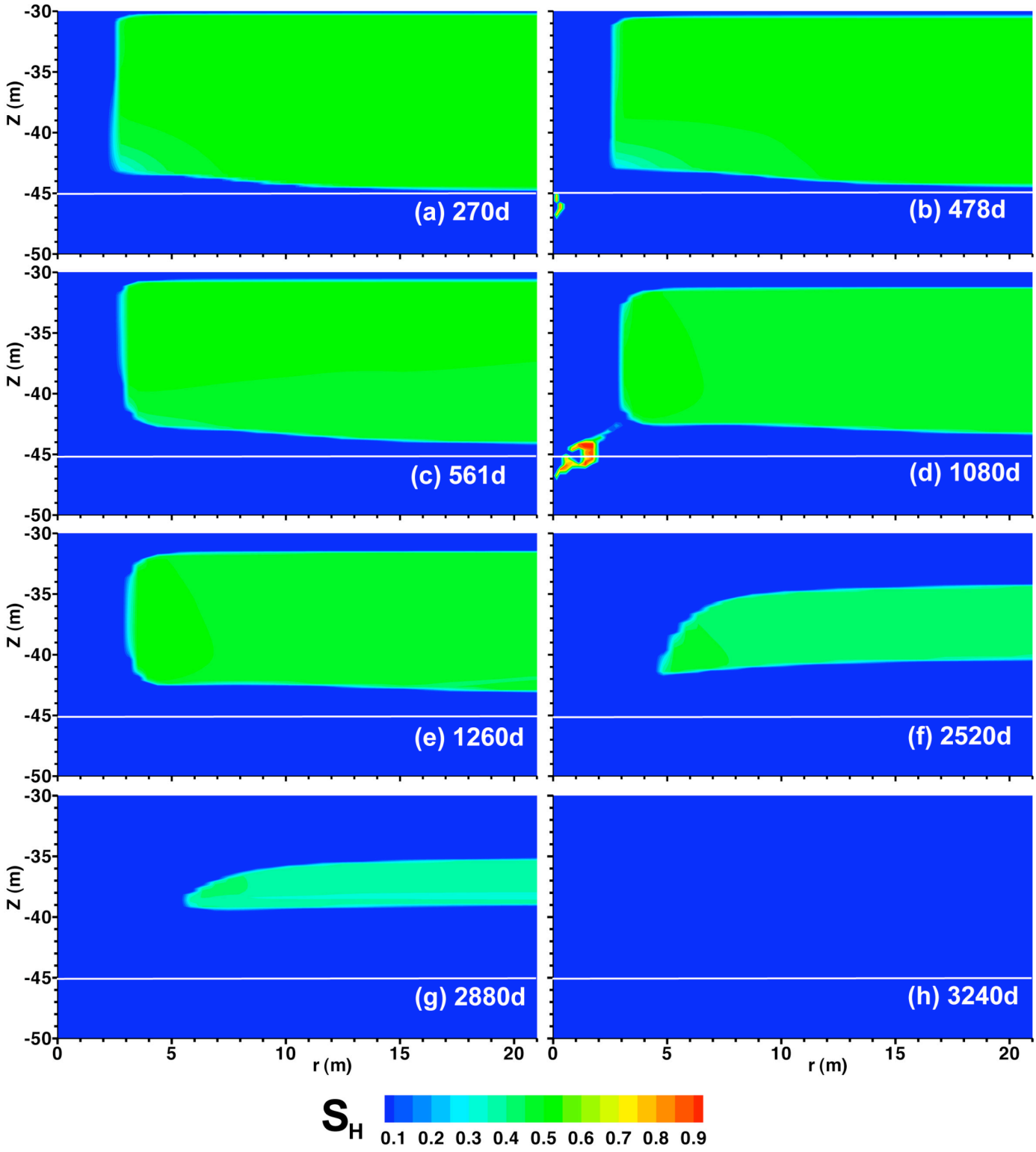

Figure 21 –Evolution of spatial distribution of S_H during gas production from the Class 2 PA hydrate deposit in Case C.

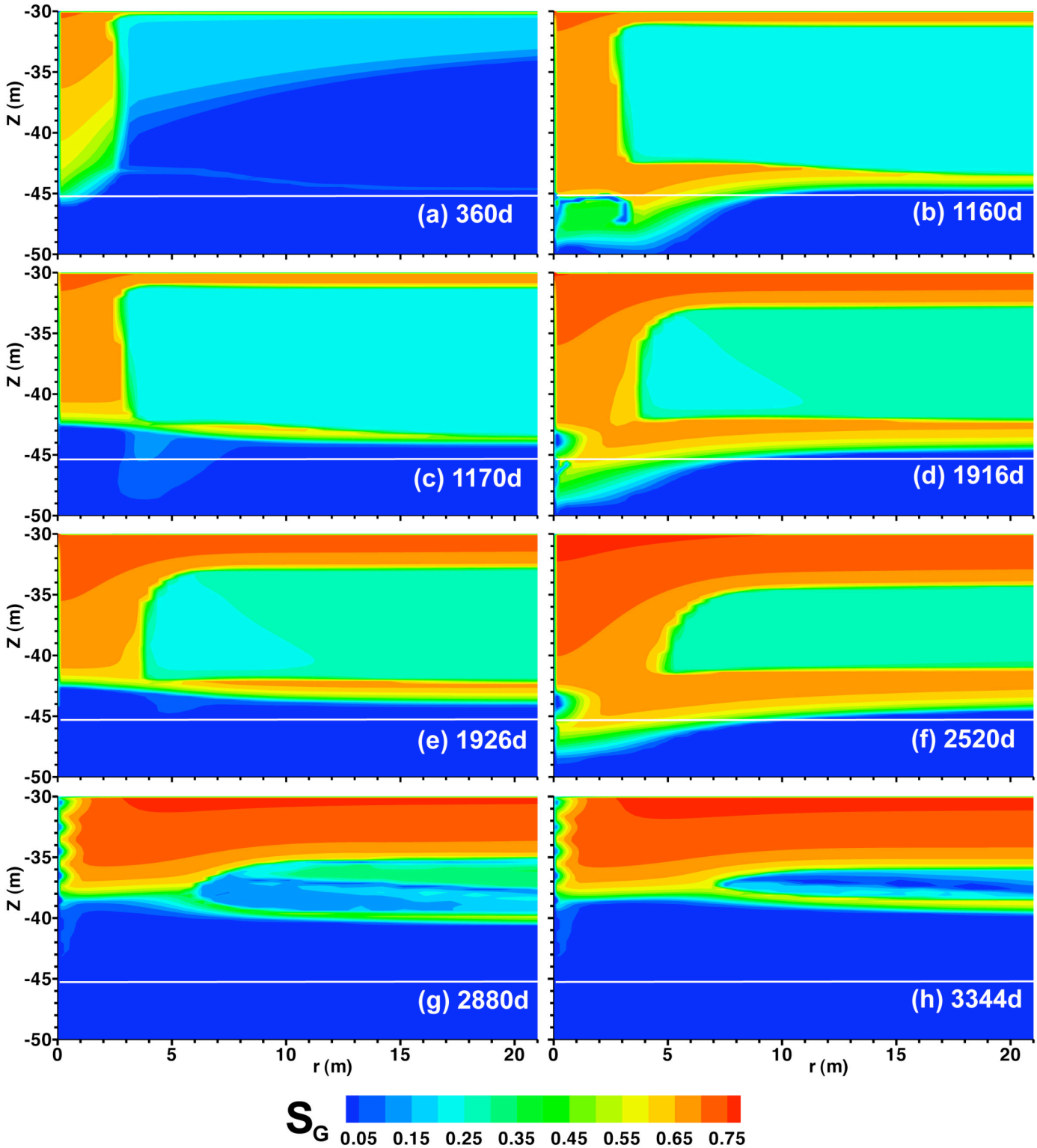

Figure 22 –Evolution of spatial distribution of S_G during gas production from the Class 2 PA hydrate deposit in Case C.

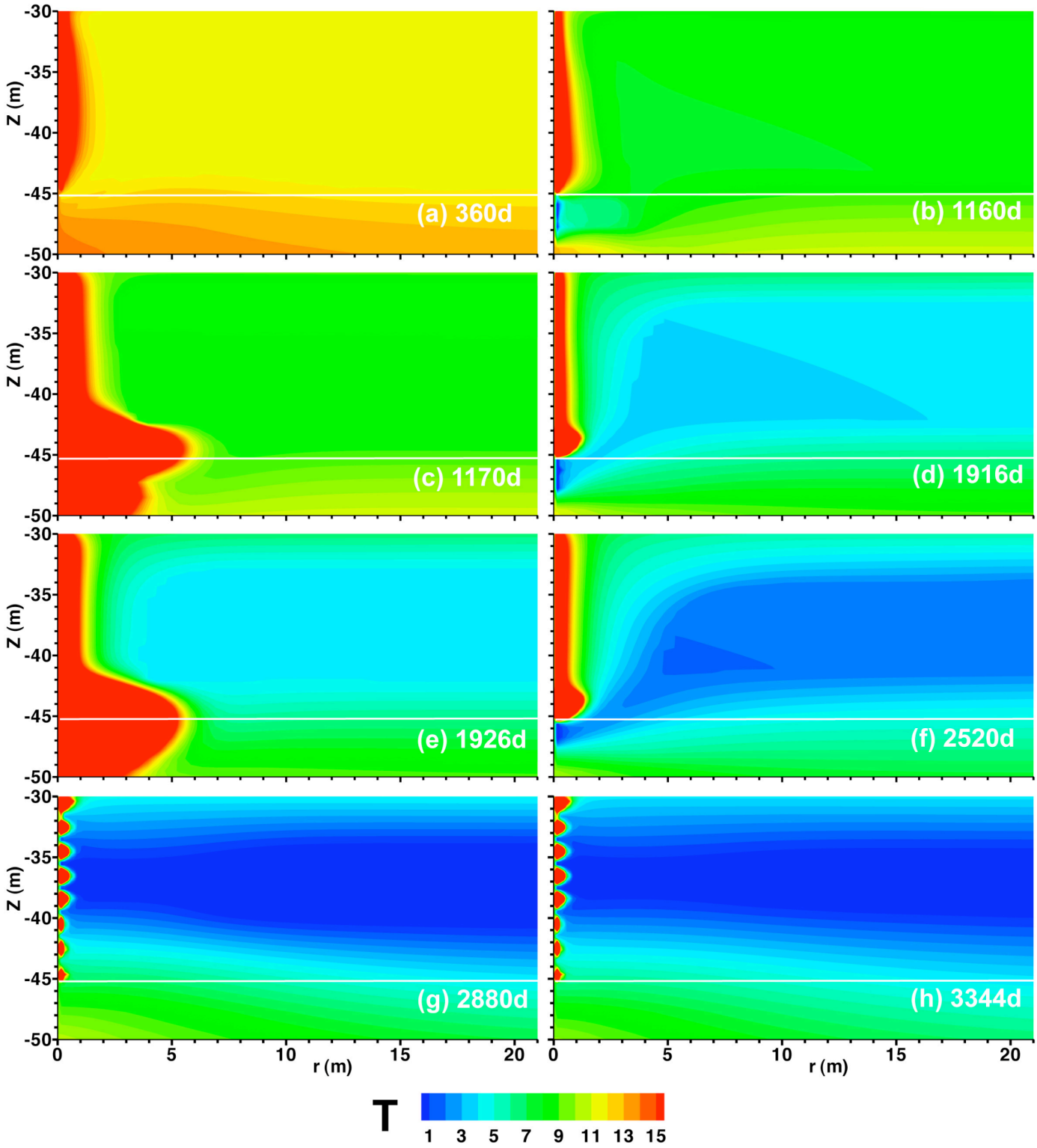

Figure 23 –Evolution of spatial distribution of T during gas production from the Class 2 PA hydrate deposit in Case C.

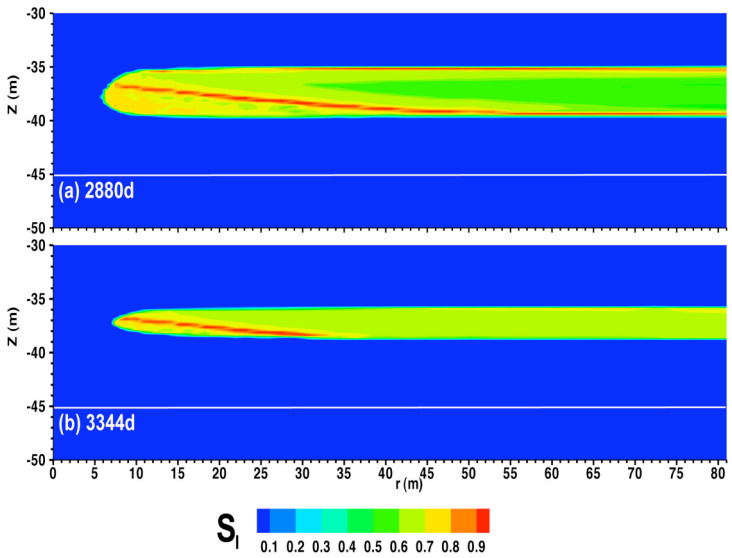

Figure 24 –Evolution of spatial distribution of S_I during gas production from the Class 2 PA hydrate deposit in Case C.

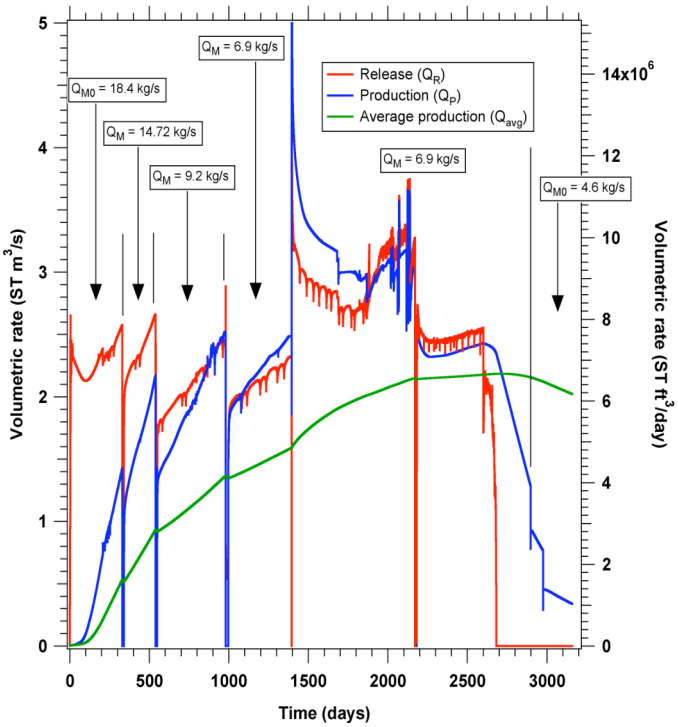

Figure 25 – Evolution of Q_R and Q_P during production from the Class 2 PA hydrate deposit in Case C for $Q_{M0} = 2Q_{M0,ref}$. The evolution of Q_M and Q_{avg} over the simulation period are also shown.

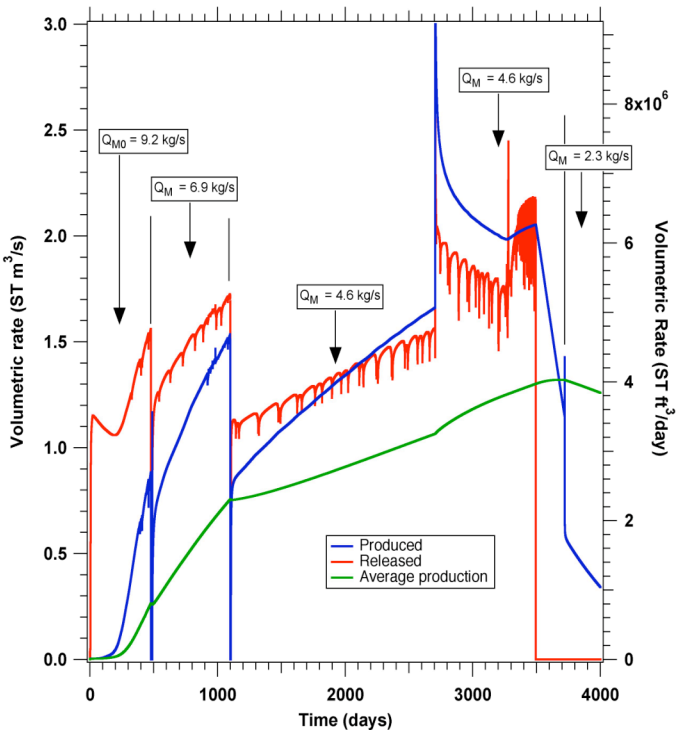

Figure 26 – Rates of (a) hydrate-originating CH_4 release in the reservoir (Q_R) and (b) CH_4 production at the well (Q_P) during production from the Class 2 PA hydrate deposit in Case C when S_H = 0.55. The average production rate (Q_{avg}) over the simulation period is also shown.

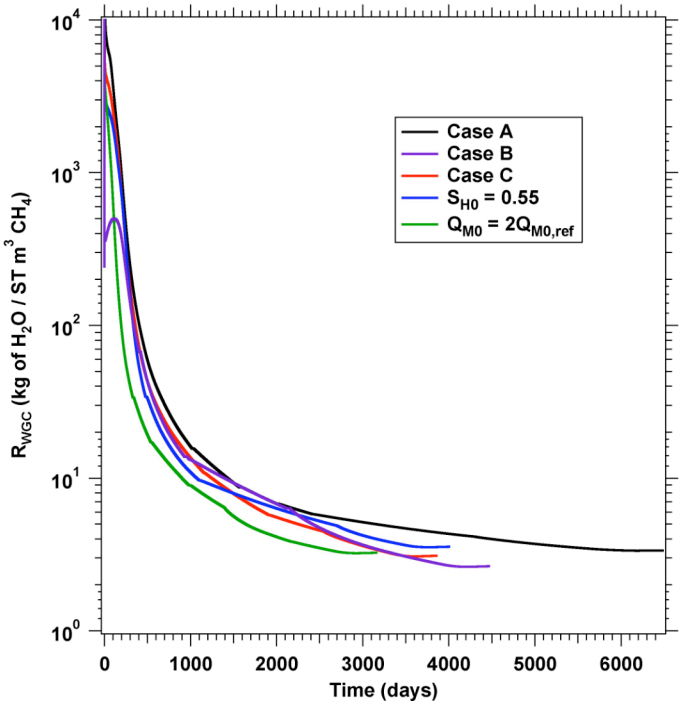

Figure 27 – Evolution of the water-to-gas ratio (R_{WGC}) over time during gas production from the PA hydrate deposit in this study. Note the continuous and monotonic decline of R_{WGC} until the time of the hydrate exhaustion.